

EGG-TMI-7825

PATENT CLEARED

C 2

EGG-TMI-7825

**INFORMAL REPORT**

PORV DISCHARGE FLOW DURING THE TMI-2 ACCIDENT

Y. Nomura

**LOAN COPY**

THIS REPORT MAY BE RECALLED  
AFTER TWO WEEKS. PLEASE  
RETURN PROMPTLY TO:

INEL TECHNICAL LIBRARY


824



**Idaho  
National  
Engineering  
Laboratory**

Managed  
by the U.S.  
Department  
of Energy



Work performed under  
DOE Contract  
No. DE-AC07-76ID01570

## DISCLAIMER

This book was prepared as an account of work sponsored by an agency of the United States Government. Neither the United States Government nor any agency thereof, nor any of their employees, makes any warranty, express or implied, or assumes any legal liability or responsibility for the accuracy, completeness, or usefulness of any information, apparatus, product or process disclosed, or represents that its use would not infringe privately owned rights. References herein to any specific commercial product, process, or service by trade name, trademark, manufacturer, or otherwise, does not necessarily constitute or imply its endorsement, recommendation, or favoring by the United States Government or any agency thereof. The views and opinions of authors expressed herein do not necessarily state or reflect those of the United States Government or any agency thereof.

**PORV DISCHARGE FLOW DURING THE TMI-2 ACCIDENT**

**Yasushi Nomura**

**Published July 1987**

**EG&G Idaho, Inc.  
Idaho Falls, Idaho 83415**

**Prepared for the  
U.S. Department of Energy  
Idaho Operations Office  
Under DOE Contract No. DE-AC07-76ID01570**



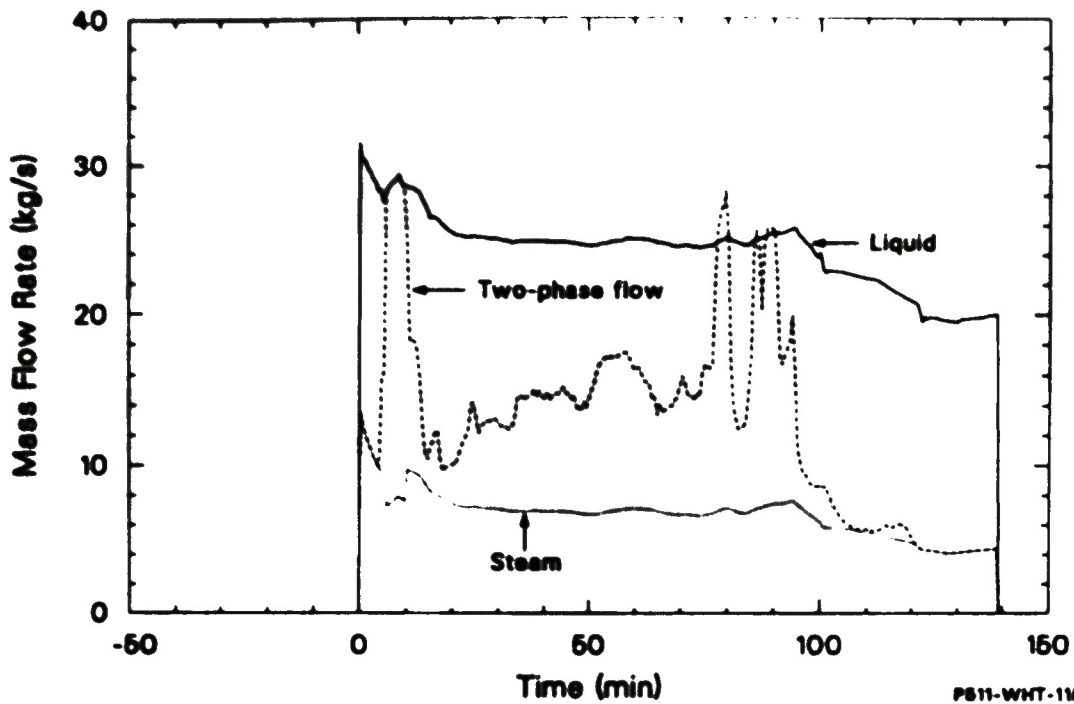
## ABSTRACT

PORV discharge flow during the TMI-2 accident was estimated by calculating the void fraction in the pressurizer based on experimental correlations (or zero void fraction when temperature and pressure measurements indicated subcooling) and critical flow through the PORV. A computer program was developed and its validity was demonstrated by comparing calculational and experimental data. Input variables, such as discharge coefficients or effluent fluid enthalpies, were carefully evaluated to assure best calculational results. A case using Wilson's correlation for the saturated pressurizer and linear interpolation in fluid enthalpy between subcooled points as indicated by measurements is considered to give the best-estimate of the total discharge from the PORV during the accident.

## SUMMARY

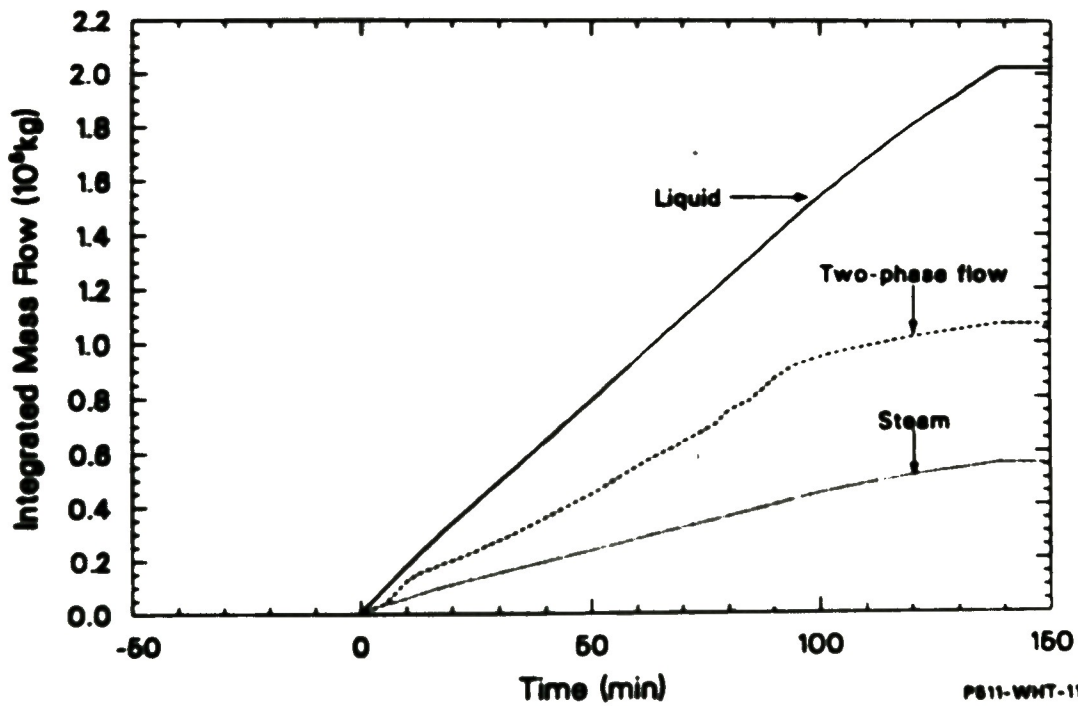
Discharge flow through the PORV during the TMI-2 accident was estimated by employing two experimental correlations, Wallis's and Wilson's, for steam velocities in the pressurizer. Davis's critical flow tables using the Henry-Fauske model for subcooled stagnation conditions and the Homogeneous Equilibrium Model for two-phase conditions were used to obtain the critical mass flux through the PORV. A computer program was developed to calculate the discharge flow through the PORV, and its validity was verified by comparing calculational and experimental data. Calculational conditions, such as discharge coefficients, for input to the computer program were investigated to estimate the PORV mass flow. Thermal hydraulic behavior related to the PORV block valve operation was surveyed to get a good estimation for mass flow.

Wilson's correlation is considered to give more reasonable steam velocities than Wallis's correlation, judging from the plant conditions during the TMI-2 accident. Figures S-1 and S-2 show calculational results from 0 to 139 min for Wilson's correlation compared with those for all-steam and all-saturated liquid. A best-estimate case, using Wilson's correlation and accounting for subcooled fluid effects after 315 min, predicts calculational results such as those shown in Figures S-3 and S-4. These results are considered to be adequate when compared to the results of other researchers.



PS11-WHT-1187-09

Figure S-1. Comparison of calculated mass-flowrates for all-steam, all-liquid, and two-phase flow by Wilson's equation.



PS11-WHT-1187-12

Figure S-2. Comparison of calculated integrated mass-flows for all-steam, all-liquid, and two-phase flow by Wilson's equation.

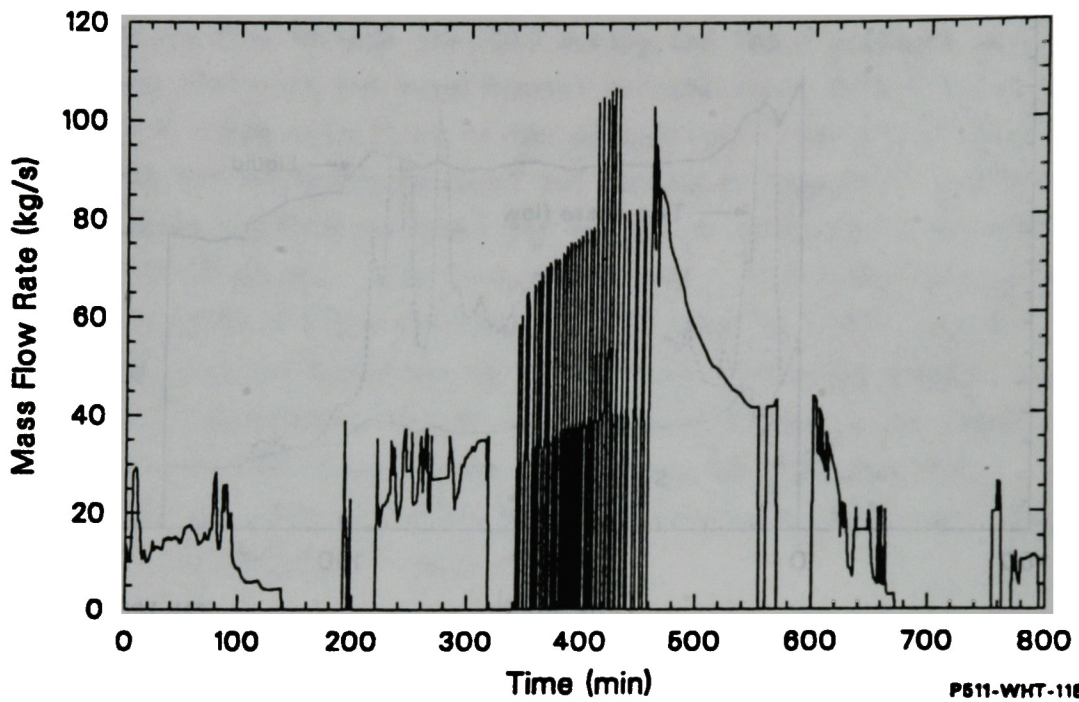


Figure S-3. Calculated mass flowrate for a best-estimate case.

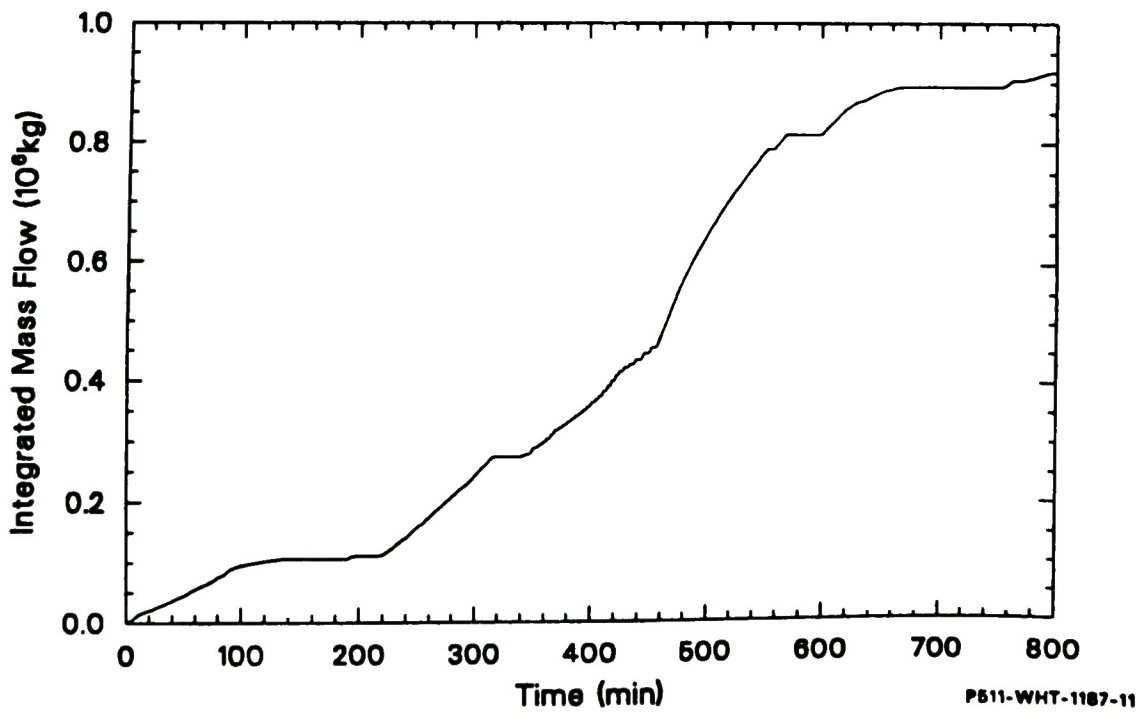


Figure S-4. Calculated integrated mass-flow for a best-estimate case.

## CONTENTS

ABSTRACT .....	11
SUMMARY .....	111
1. INTRODUCTION .....	1
2. CALCULATIONAL METHOD .....	3
2.1 Critical Flow Model .....	3
2.2 Calculational Method for Discharge Flow .....	5
3. PROGRAM VERIFICATION WITH EXPERIMENTAL DATA .....	10
3.1 System Description of the Experiment .....	10
3.2 Test Sequence and System Response .....	10
3.3 Verification of Computer Program .....	18
4. CALCULATIONAL CONDITIONS FOR DISCHARGE FLOW .....	24
4.1 TMI-2 Plant System Configuration .....	24
4.2 PORV Throat Area and Discharge Coefficient .....	24
4.3 Operation of PORV and Thermal Hydraulic Transient .....	29
5. CALCULATIONAL RESULTS AND THEIR ASSESSMENT .....	39
5.1 Comparison of Saturation Model and Subcooled Model .....	39
5.2 Comparison of Wallis's and Wilson's Equation .....	39
5.3 A Maximum Flow Limiting Case .....	43
5.4 A Best-Estimate Case .....	46
6. UNCERTAINTY ANALYSIS .....	49
7. CONCLUSIONS .....	50
8. REFERENCES .....	51

## FIGURES

S-1. Comparison of calculated mass-flowrates for all-steam, all-liquid, and two-phase flow by Wilson's equation .....	iv
--	----

S-2. Comparison of calculated integrated mass-flows for all-steam, all-liquid, and two-phase flow by Wilson's equation .....	1v
S-3. Calculated mass flowrate for a best-estimate case .....	v
S-4. Calculated integrated mass-flow for a best-estimate case .....	v
1. Comparison of critical flow models .....	4
2. Schematic of bubble flow in the pressurizer .....	7
3. Calculational flow diagram for discharge flowrate .....	9
4. Isometric configuration for Semiscale Test S-PL-3 .....	11
5. Schematic configuration of Semiscale Test S-PL-3 .....	12
6. Primary system pressure from Semiscale Test S-PL-3 .....	17
7. HPIS charging and PORV leakage flowrates from Semiscale Test S-PL-3 .....	17
8. Calculated mass flowrate through PORV by the saturation model with Wilson's correlation .....	19
9. Experimental mass flowrate through the PORV .....	19
10. Comparison of calculated results with experimental data (1) .....	20
11. Measured fluid temperature and saturation temperature in the pressurizer .....	20
12. Comparison of calculated results with experimental data (2) .....	21
13. Comparison of calculated results for total mass loss with experimental data .....	23
14. TMI-2 reactor coolant system showing main components .....	25
15. Longitudinal cut-out view of the pressurizer .....	26
16. Pressurizer level and primary system pressure .....	30
17. A-loop hot leg, cold leg, and saturation temperatures (1) .....	32
18. A-loop hot leg, cold leg, and saturation temperatures (2) .....	32
19. A-loop hot leg, cold leg, and saturation temperatures (3) .....	34
20. Comparison of pressurizer liquid level and primary system pressure (1) .....	34

21.	Comparison of pressurizer liquid level and primary system pressure (2) .....	35
22.	Comparison of system temperatures (A-loop hot and cold and PZR) with saturation .....	37
23.	Calculated mass flowrate through PORV by the saturation model ....	40
24.	Calculated mass flowrate through PORV by the subcooled model .....	40
25.	Comparison between integrated mass-flows by the saturation and subcooled models .....	41
26.	Calculated PORV void-fractions by Wilson's and Wallis's correlations .....	41
27.	Comparison of calculated mass flowrates for all-steam, all-liquid, and two-phase flow by Wilson's and Wallis's equations .....	42
28.	Comparison of integrated mass-flow calculated by Wilson's and Wallis's equations .....	44
29.	Calculated mass flowrate by Wilson's equation .....	44
30.	Calculated mass flowrate by Wallis's equation .....	45
31.	Comparison of integrated mass-flow calculated by Wilson's and Wallis's equations .....	45
32.	Comparison of calculated integrated mass-flow between the best estimate case and the limiting case .....	47
33.	Calculated mass flowrates for the best estimate case .....	47
34.	Calculated mass flowrates for the limiting case .....	48

#### TABLES

1.	Conditions at transient initiation--Test S-PL-3 .....	13
2.	Primary coolant temperature distribution before transient .....	14
3.	Sequence of events .....	16
4.	EPRI Dresser Model 31533VX-30 valve flow tests .....	28
5.	PORV block valve opening and closing times .....	38



## PORV DISCHARGE FLOW DURING THE TMI-2 ACCIDENT

### 1. INTRODUCTION

The loss of fluid from the reactor coolant system (RCS) was the key factor leading to core degradation during the TMI-2 accident on March 28, 1979. During the TMI-2 accident, about half of the primary system coolant was lost to the containment building over approximately the first two and a half hours through a stuck-open Pilot Operated Relief Valve (PORV) on the pressurizer. At approximately 100 min into the accident, the last set of Reactor Coolant Pumps (RCP) were tripped allowing the remaining primary coolant to stratify. As a result, limited water inventory was available to maintain core cooling, and within minutes the top of the core was uncovered and began to overheat, resulting in core damage. The severe core damage continued until after 200 min into the accident when high pressure injection was started and a significant quantity of water was added to the core, resulting in a covered core by approximately 207 min.

Although the accident has enhanced the understanding of core damage progression in a commercial pressurized light water reactor in a loss-of-coolant accident, many important data were not recorded by plant instrumentation that was intended for normal reactor operations. One set of important data not recorded was the loss of fluid through the PORV during the accident. The precise leakage flowrate data are required, for instance, to estimate the make-up or High Pressure Injection (HPI) flowrates (another parameter which was not recorded) for use as a critical boundary condition for the severe accident analysis codes such as SCDAP/RELAP5.<sup>1</sup>

This document presents estimated leakage fluid-flow through the PORV during the first 800 min of the accident. The purpose is to give the best estimation of the leakage fluid-flow for use in an international analysis exercise organized to evaluate the capabilities of the severe accident computer codes. The estimation employs the best thermal hydraulic models available at this time. Chapter 2 details the calculational method used to estimate the leakage flowrate. Chapter 3 explains the experimental data to

be used for the code verification, together with the verification results. Chapter 4 gives calculational conditions used for the leakage flow estimation, together with a brief explanation of the RCS behavior concerning the present work. Chapter 5 presents the calculated results of the PORV flowrates and accumulated leakage flow in the containment building during the accident, together with an assessment of the calculations. Finally, Chapter 6 provides a discussion of the uncertainty of estimation, and Chapter 7 gives our conclusions.

## 2. CALCULATIONAL METHOD

### 2.1 Critical Flow Model

If the effluent fluid is comprised of single-phase steam, the flowrate is generally estimated by the following isentropic-flow equation for a compressible fluid,

$$W = C_d \cdot A \cdot [2\gamma/(\gamma - 1) \cdot \rho_g \cdot P_0 \cdot (\eta^{2/\gamma} - \eta^{1 + 1/\gamma})]^{1/2} \quad (1)$$

where  $C_d$  is the discharge coefficient,  $A$  is the throat area,  $\gamma$  is the specific heat ratio,  $\rho_g$  is the steam density,  $P_0$  is the upstream stagnation pressure, and  $\eta$  is the critical pressure ratio. The term  $\eta$  is the ratio of throat pressure to upstream stagnation pressure, and, for an ideal gas, it is given by;

$$\eta = [2/(\gamma + 1)]^{\gamma/(\gamma - 1)} \quad (2)$$

At the rated conditions of the TMI-2 PORV, with  $\gamma = 1.25$  and  $\eta = 0.555$ , Eq. (1) yields a compressible discharge coefficient of 0.77 for the PORV.<sup>2</sup> This value lies between 0.61, which is the value for a sharp-edged orifice, and 1.0, which is the value for an ideal nozzle.

If the effluent fluid is a saturated two-phase mixture, the discharge flowrate can be evaluated using critical flow models such as the homogeneous equilibrium model (HEM), Henry-Fauske model (HFM), and the Moody model. Figure 1 illustrates the critical mass flux calculated from these models as a function of upstream stagnation enthalpy for three different pressures.<sup>2</sup> In general, HEM yields the lowest discharge rate and the Moody model predicts the highest flowrate except near saturated liquid enthalpy.

If the effluent flow is subcooled liquid, the discharge flowrate can be given by the incompressible Bernoulli's equation as follows:



$$W = C_d^d \cdot A \cdot [2 \rho_f \cdot P_0 \cdot (1 - \eta)]^{1/2} \quad (3)$$

To estimate leakage flowrate through the PORV during the TMI-2 accident, the critical flow tables developed by C. Davis,<sup>3</sup> are used, together with the application program. Critical mass flux is then calculated based on a combination of HFM and HEM. This combination of critical flow models was found to generally give good agreement with data when the RELAP4 thermal-hydraulic computer code was assessed. The program uses HFM for subcooled stagnation conditions and HEM for two-phase conditions. A linear interpolation between the two models is used between 0 and 2% quality.

## 2.2 Calculational Method for Discharge Flow

For the purpose of estimating discharge flow through the PORV, many researchers have used the premise that void fraction at upstream stagnation is equal to that in the pressurizer.<sup>2</sup> For greater accuracy, critical discharge flow through the narrow orifice of the PORV should be determined as a function of pressure, temperature, and quality of upstream stagnation, which are different from those present in the pressurizer. On the other hand, steam flowrate through the pressurizer should be determined as a function of fluid properties, including void fraction in the pressurizer.

There are some experimentally deduced steam-velocity equations applicable to the condition of the pressurizer. Wallis's equation<sup>4</sup> is one of those, and is described as follows:

$$j_{go} = 1.53 \cdot \alpha(1 - \alpha) \cdot [\sigma \cdot G \cdot (\rho_f - \rho_g) / \rho_f^2]^{1/4} \quad (4)$$

where  $\alpha$  is void fraction,  $\sigma$  is surface tension,  $G$  is the gravity constant,  $\rho_f$  is liquid density, and  $\rho_g$  is vapor density.

The above equation can be applied for bubbly flow of rather low quality. Wilson<sup>5</sup> developed a void fraction correlation based upon experimental data obtained by bubbling saturated steam through saturated

liquid in a 19-in. diameter vessel at pressures up to 600 psig. A manometer was used to measure the void fraction in the vessel, below the interface level. Because this configuration is very close to the TMI-2 pressurizer configuration, Wilson's equation might give good correlation as follows.

$$j_{go} = [\alpha/C_1 \cdot (\Delta\rho/\rho_g)^{C_2} \cdot (D_e^2 \cdot G \cdot \Delta\rho/\sigma)^{C_4/2} ]^{1/C_3} \cdot (\sigma \cdot G \cdot \Delta\rho/\rho_f^2)^{1/4} \quad (5)$$

where  $\Delta\rho$  is  $\rho_f - \rho_g$ ,  $C_1$  is 0.546,  $C_2$  is 0.12,  $C_3$  is 0.67 and  $C_4$  is 0.1.  $D_e$  is the equivalent diameter, which is four times the flow-area divided by the wetted periphery.

Bubbly flow in the pressurizer is schematically shown in Figure 2. The level of the collapsed liquid can be measured by the difference between the hydrostatic heads of the fluid columns in the reference leg and the pressurizer. Void fraction in the pressurizer can be obtained by the following equation with the measured liquid level.

$$\alpha = 1.0 - L_{str}/L_{ful} \quad (6)$$

where  $L_{str}$  is measured liquid level and  $L_{ful}$  is full-scale level (the vertical distance between taps; 400 in.).

As seen in Figure 2, for a less-than-full pressurizer (in the case of bubbly flow), steam must be separated from water in the upper region of the pressurizer to go through the PORV. In this situation, steam flow deduced from either Eq. (4) or Eq. (5) must be less than or equal to critical steam flow through the PORV, since the critical flow-rate is the maximum possible flow-rate through the PORV.

To estimate the discharge flowrate through the PORV, steam flowrate is first obtained by Wilson's equation or Wallis's equation. Then discharge

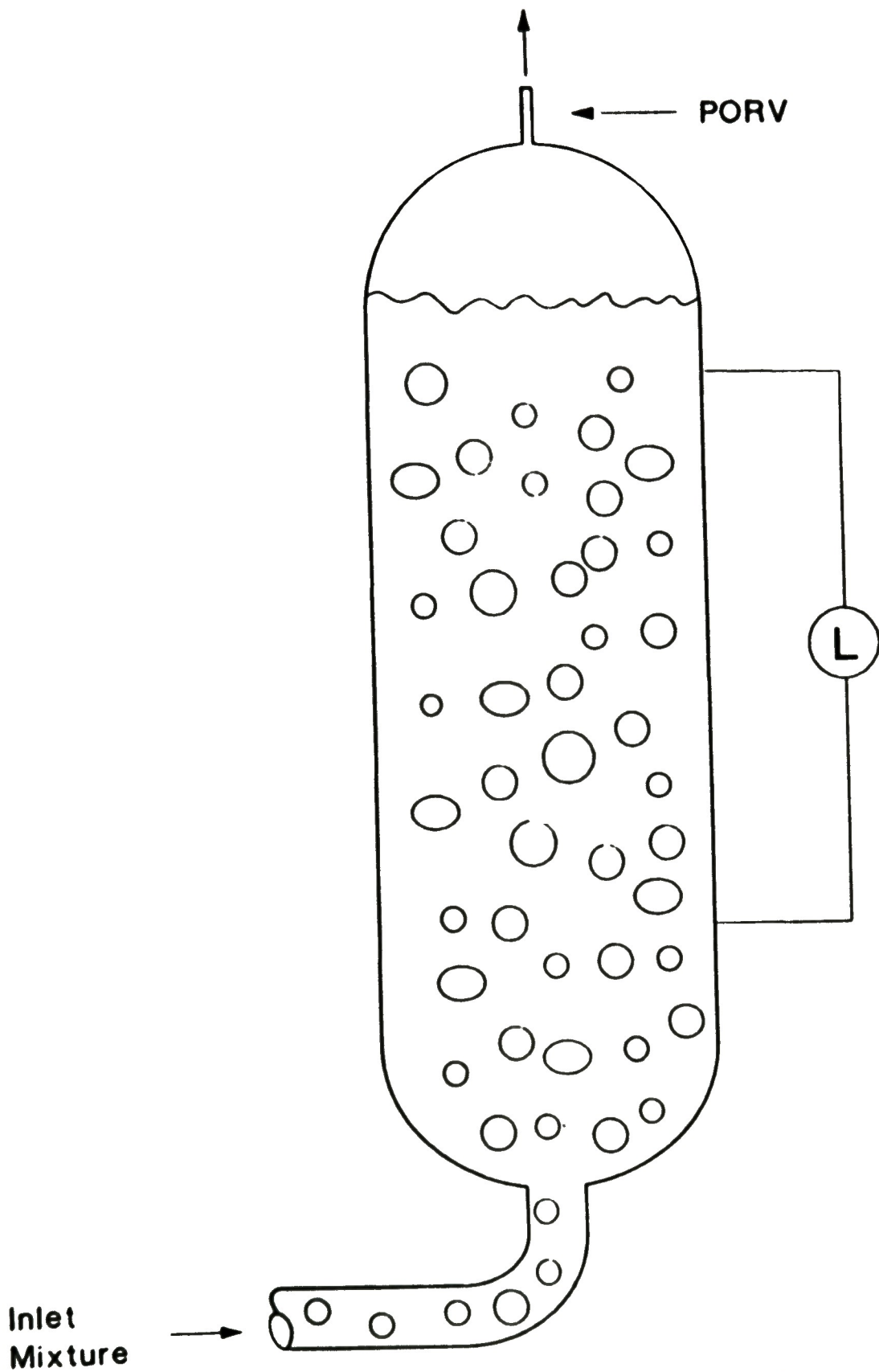


Figure 2. Schematic of bubble flow in the pressurizer.

fluid flowrate is determined from the Davis critical flow tables using upstream pressure, enthalpy, and steam velocity. Figure 3 shows a calculational flow-diagram for estimating the PORV discharge flowrate.

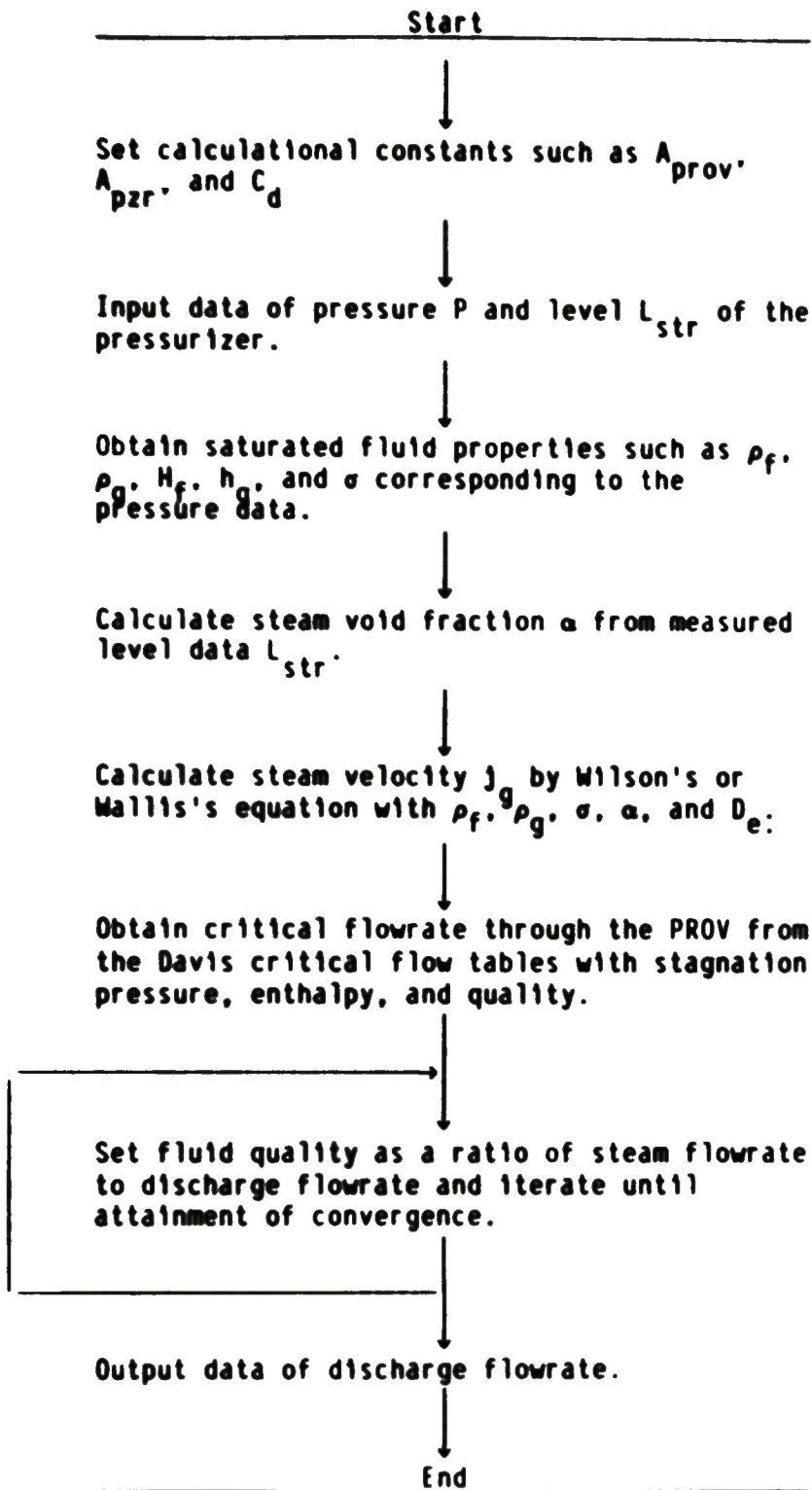


Figure 3. Calculational flow diagram for discharge flowrate.



### 3. PROGRAM VERIFICATION WITH EXPERIMENTAL DATA

A computer program has been developed to calculate the discharge flowrate through the PORV according to the calculational method described in the previous chapter. Verification of the program with experimental data is presented in this chapter.

#### 3.1 System Description of the Experiment<sup>6</sup>

A series of tests named the Semiscale Mod-2B Power Loss Experiment (S-PL-1, -2, and -3) was conducted by EG&G Idaho, Inc., on November 31, December 14, 1982, and March 1, 1983, respectively. S-PL-3 simulated a loss-of-offsite power transient with accompanying failures of the auxiliary feedwater and emergency AC power systems. The primary objective of these tests was to provide a data base on general plant response during loss-of-offsite power transients. Data from the S-PL-3 experiment is used for assessment of the previously described method for calculation of critical flow through the pressurizer PORV.

The Semiscale Mod-2B system is equipped with a pressure vessel that contains an electrically heated core, other simulated reactor internals, and an external downcomer assembly; an intact loop with a pressurizer, a steam generator, and a primary pump; a broken loop with a steam generator, a primary pump, and a rupture assembly. Configuration of the experimental system is shown in Figures 4 and 5. High-pressure coolant injection pumps (HPIS) were provided for both loops. These pumps, coupled with a power operated relief valve (PORV) on the pressurizer, enabled the feed and bleed recovery. The intact loop is scaled to represent three of the four primary loops in a Westinghouse-designed PWR, while the broken loop represents the fourth. Even though S-PL-3 does not incorporate a break in either loop, the second loop is still referred to as the "broken loop."

#### 3.2 Test Sequence and General System Response<sup>7</sup>

Tables 1 and 2 show conditions in the Semiscale Mod-2B system at transient initiation (from Ref. 7). Experimental sequence of events can be

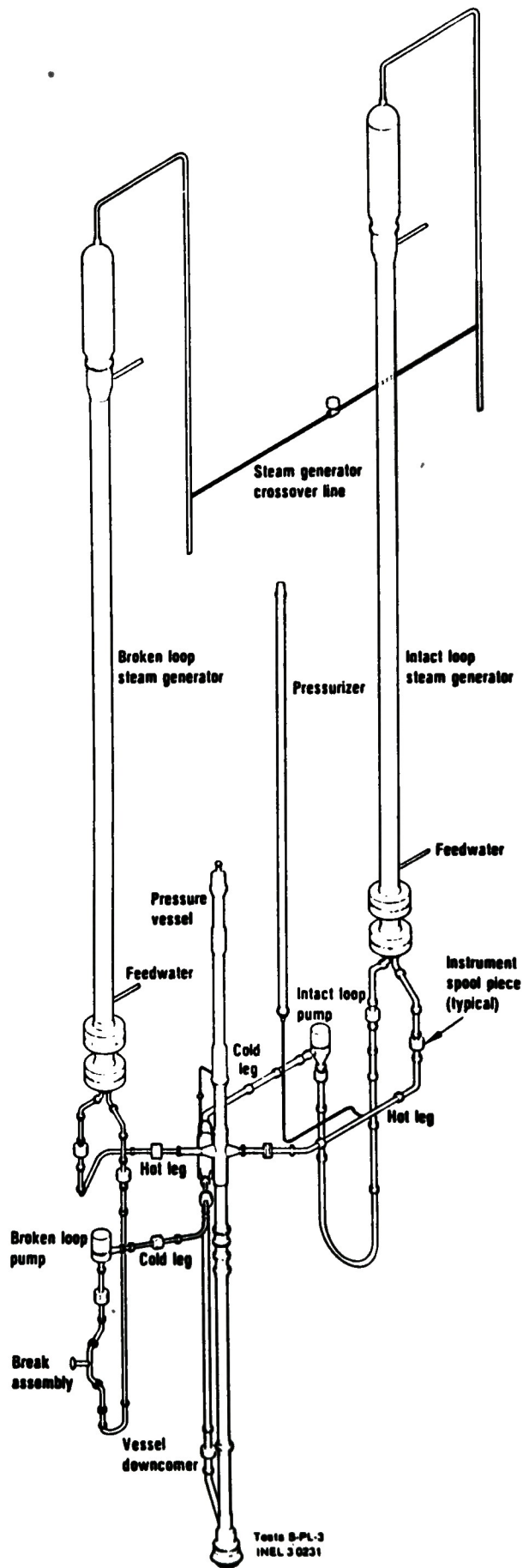


Figure 4. Isometric configuration for Semiscale Test S-PL-3.

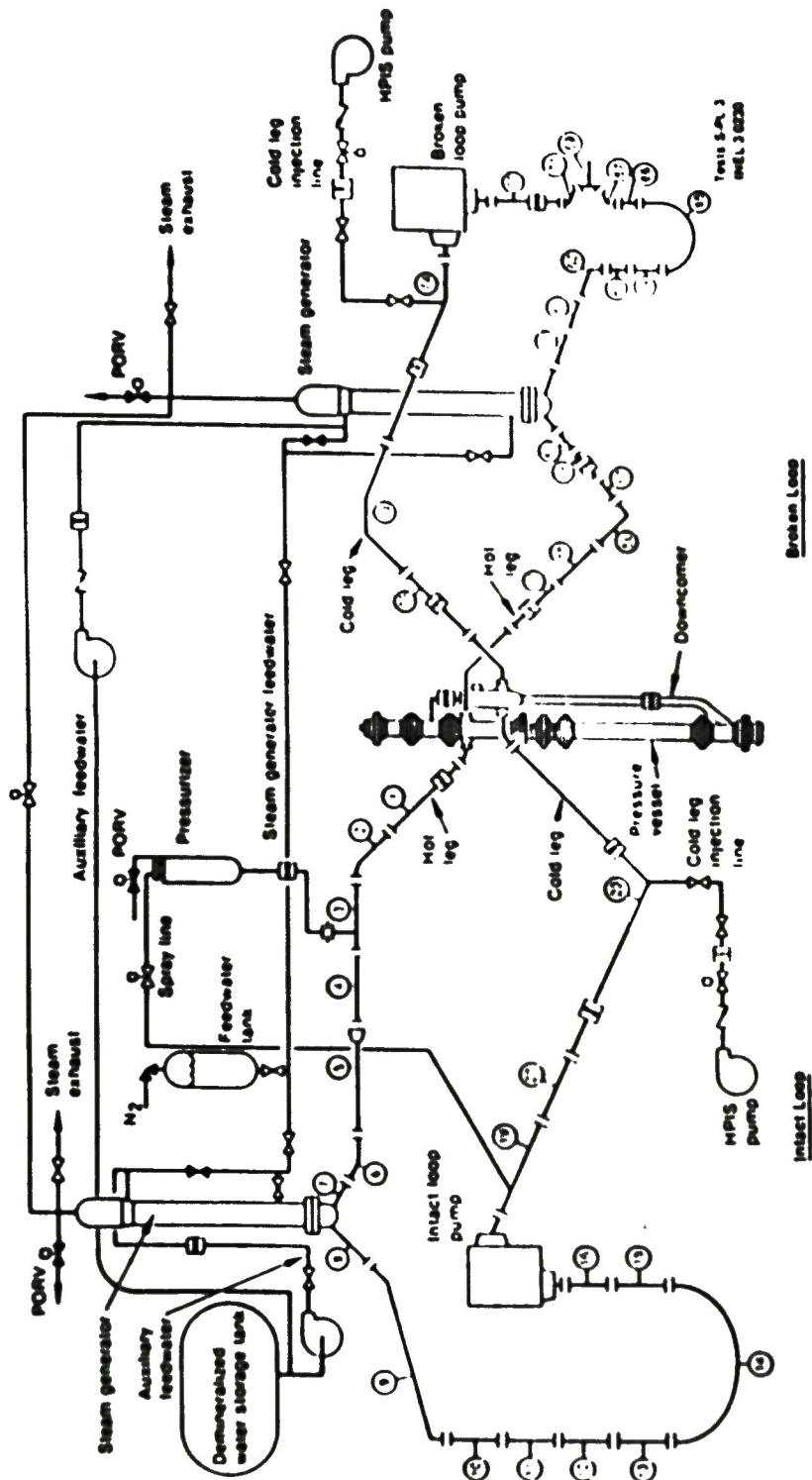


Figure 5. Schematic configuration of Semiscale Test S-PL-3.

TABLE 1. CONDITIONS AT TRANSIENT INITIATION--TEST S-PL-3

	<u>Measured<sup>a</sup></u>	<u>Specified</u>
Core power, MW	2.096	2.18 ± 0.05 MW
System pressure, MPa (psia) <sup>b</sup>	15.2 (2205)	14.8 ± 0.2 MPa (2146.6 ± 29 psia)
Intact loop cold leg fluid temperature, K (°F)	571 (568)	567 ± 2 K (561 + 4°F)
Broken loop cold leg fluid temperature, K (°F)	568 (563)	567 ± 2 K (561 ± 4°F)
Intact loop hot leg to cold leg temperature differential, K (°F)	34.4 (62.0)	38 ± 2 K (68 ± 4°F)
Broken loop hot leg to cold leg temperature differential, K (°F)	36.3 (65.3)	38 ± 2 K (68 ± 4°F)
Intact loop cold leg flow, L/s (gpm)	9.69 (153.6)	9.7 ± 0.1 L/S (1537 ± 2 gpm)
Broken loop cold leg flow, L/s (gpm)	3.18 (50.4)	3.2 ± 0.1 L/s (50.7 ± 2 gpm)
Pressurizer fluid level, cm (in.)	263 (103.3) 439 (127.9)	215 ± 5 cm, cold 358.7 cm, (141.2 in., hot)
Steam generator feedwater temperature, K (°F)	512 (562)	495 ± 2 K (431 ± 4°F) <sup>c</sup>
Intact loop steam generator liquid mass, kg (lb)	60 (133) <sup>d</sup>	78.5 ± 1 kg (173 ± 2 lb) <sup>c</sup>
Broken loop steam generator liquid mass, kg (lb)	27.5 (60.8) <sup>d</sup>	26.2 ± 1 kg (58 ± 2 lb) <sup>e</sup>

a. Measured initial conditions are taken from digital data acquisition system reading prior to transient initiation.

b. parenthetical expressions and number are English units.

c. One source of feedwater for intact and broken loops.

d. Measurement taken 20 s after transient initiation.

e. The steam generator liquid levels were adjusted to achieve the required differential temperature across the core.

TABLE 2. PRIMARY COOLANT TEMPERATURE DISTRIBUTION BEFORE TRANSIENT<sup>a</sup>

	Detector	Temperature K (°F)		
		Test S-PL-1	Test S-PL-2	Test S-PL-3
Intact loop hot leg (near vessel)	TFI*1	587 (597) <sup>b</sup>	584 (591)	605 (629)
Intact loop cold leg (pump suction)	TFI*9	551 (532)	550 (530)	571 (568)
Intact cold leg (near downcomer)	TFI*22	550 (530)	549 (528)	--
Intact loop cold leg (near downcomer)	TFI*238B	--	--	571 (568)
Broken loop hot leg (near vessel)	TFB*50	586 (595)	584 (591)	604 (627)
Broken loop cold leg (near downcomer)	TFB*79	554 (537)	551 (532)	568 (563)
Core (top of heated length)	TFV*A4+366	590 (602)	587 (597)	606 (631)
Core (middle of heated length)	TFV*B3+166	572 (570)	569 (564)	587 (597)
Core (bottom of heated length)	TFV*B3+46	552 (534)	551 (532)	570 (566)
Vessel lower plenum	TFV*LP-522	546 (523)	551 (532)	570 (566)

a. Average of data taken from -30 to -10 s before transient initiation.

b. Parenthetical temperatures in °F.

found in Table 3. The experiment was initiated by closing the main steam valve on both steam generators, followed by coastdown of the primary coolant pumps. The decreased primary-to-secondary heat transfer, along with the sustained core power (scram was not initiated until 5.2 s as specified), resulted in an initial primary system temperature increase and pressurization as shown in Figure 6. From scram initiation, power to the electrically heated core was automatically controlled to simulate the thermal decay response of nuclear fuel rods. Natural circulation was established by 160 s and resulted in primary system cooling and depressurization until some 2000 s. The intact loop steam generator boiled dry at 2100 s and the secondary side of the broken loop steam generator was drained at the same time. Consequently, due to the loss of secondary heat sink, primary temperatures and pressures rapidly increased until the primary code safety valve set-point [15.9 MPa (2306 psi)] was reached at 4117 s. The code safety valve began cycling and held primary pressure at 15.9 MPa for 100 s at which time the PORV was latched open and HPIS charging flow initiated. The initial flowrate through the PORV greatly exceeded the HPIS charging flow as shown in Figure 7. This, coupled with liquid holdup in the steam generator U-tubes, resulted in enough mass loss from the system to uncover the core and was followed by several distinct heater rod temperature excursion cycles. This effect is also observed in Figure 6 from roughly 6000 s to 8500 s.

The gradual drop in system pressure due to mass lost through the PORV allowed the HPIS charging mass flowrate to increase and a gradual refill of the vessel took place. At 12,000 s, a quasi-steady-state condition was reached, resulting in constant primary temperature and pressure. The oscillations occurring after 12,000 s were caused by condensation in the broken loop steam generator U-tubes. The test was terminated at 17,500 s into the transient.

TABLE 3. SEQUENCE OF EVENTS

Event	Time Relative to Transient (s)		
	S-PL-1	S-PL-2	S-PL-3
Core power level established	-527	-765	-520
Loss of offsite ac power	0	0	0
Main steam valves start to close	0	0	0
IL and BL pump coastdown initiated	2.0	2.6	2.87
Feedwater to IL and BL steam generators tripped off	2.0	2.9	2.2
SCRAM (core power decay transient started)	5.3	5.2	5.2
Emergency power established	27.0	--	--
Auxiliary feedwater available for injection	27.0	--	--
Steam generator relief valves initially opens			
Intact loop	1,950	1,584	225
Broken loop	2,126	1,814	234
Auxiliary feedwater initiated	3,246.0	--	--
Pressurizer liquid full	--	7,844	4,117
Pressurizer relief valve initially opens	--	7,844	4,117
Feed and bleed recovery procedure initiated			
PORV latches open	--	--	4,217
HPIS/charging initiated	--	--	4,217
Initial core temperature excursion	--	10,589	--
Test terminated	4,900	10,800	17,500

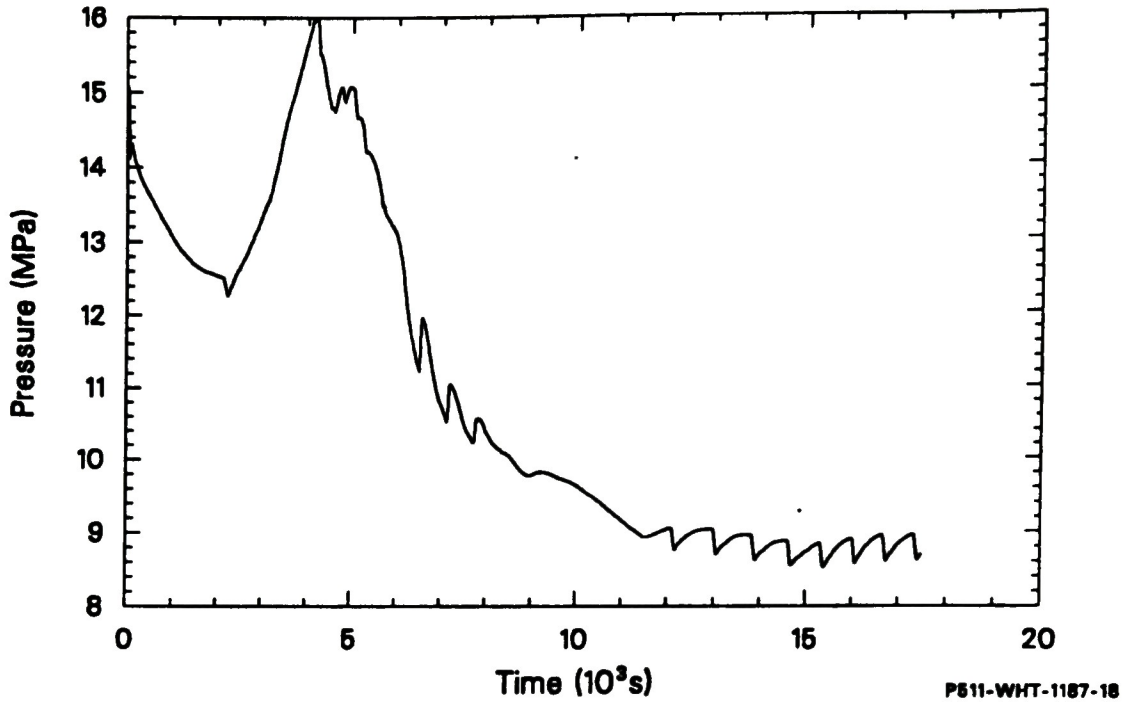


Figure 6. Primary system pressure from Semiscale Test S-PL-3.

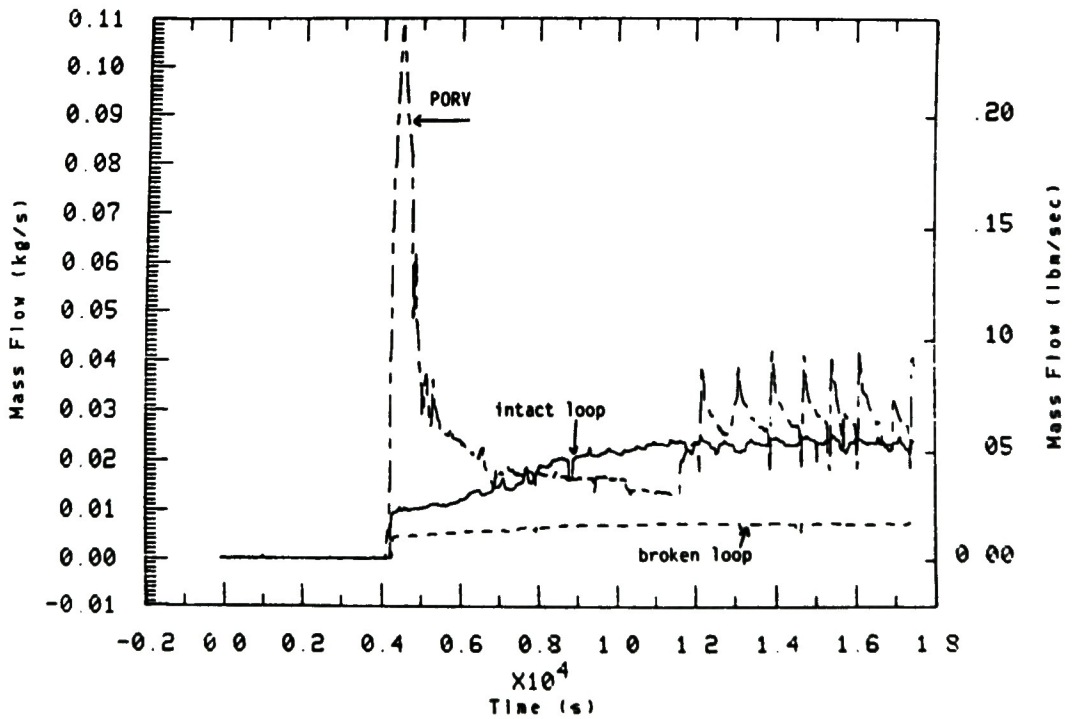


Figure 7. HPIS charging and PORV leakage flowrates from Semiscale Test S-PL-3.

### 3.3 Verification of Computer Program

Calculational conditions for verification of the program using the Semiscale data are as follows:

- throat area of the PORV ( $A_{\text{PROV}}$ ) =  $1.617 \times 10^{-6} \text{ m}^2$ ,
- inner area of the pressurizer ( $A_{\text{pZR}}$ ) =  $6.68 \times 10^{-3} \text{ m}^2$ ,
- discharge coefficients ( $C_d$ ) = 0.600 for subcooled flow and 0.787 for saturated flow, and
- full-scale level ( $L_{\text{ful}}$ ) = 6.32 m.

The above discharge coefficients were derived from some experiments explained in the next chapter.

Figure 8 shows calculated mass flowrates through the PORV for the experimental data shown in Figure 9. Wilson's equation was used to obtain steam velocity in this calculation. The agreement is good except during an initial peak-flow period as shown in the superposing plot of Figure 10.

In the period between 4250 s and 4760 s, the measured flowrate shows a sharp peak whereas the calculation gives a low flat-head shape. This difference is considered to come from incomplete modeling in the calculation. One of the errors is that the calculation assumes saturation in the pressurizer as shown in Figure 3. In fact, at the beginning period when the PORV was latched open and cool water from the RCS entered the pressurizer through the surge-line, the upstream condition of the PORV should be assumed to be subcooled. This is evident from the measured fluid temperature of the pressurizer shown in Figure 11.

The calculation program, modified with a subcooled-calculation routine using the measured pressurizer fluid-temperature for the beginning period, predicts a sharp rise in mass flowrate as shown in Figure 12. However, differences in peak values still exist between the experiment and the

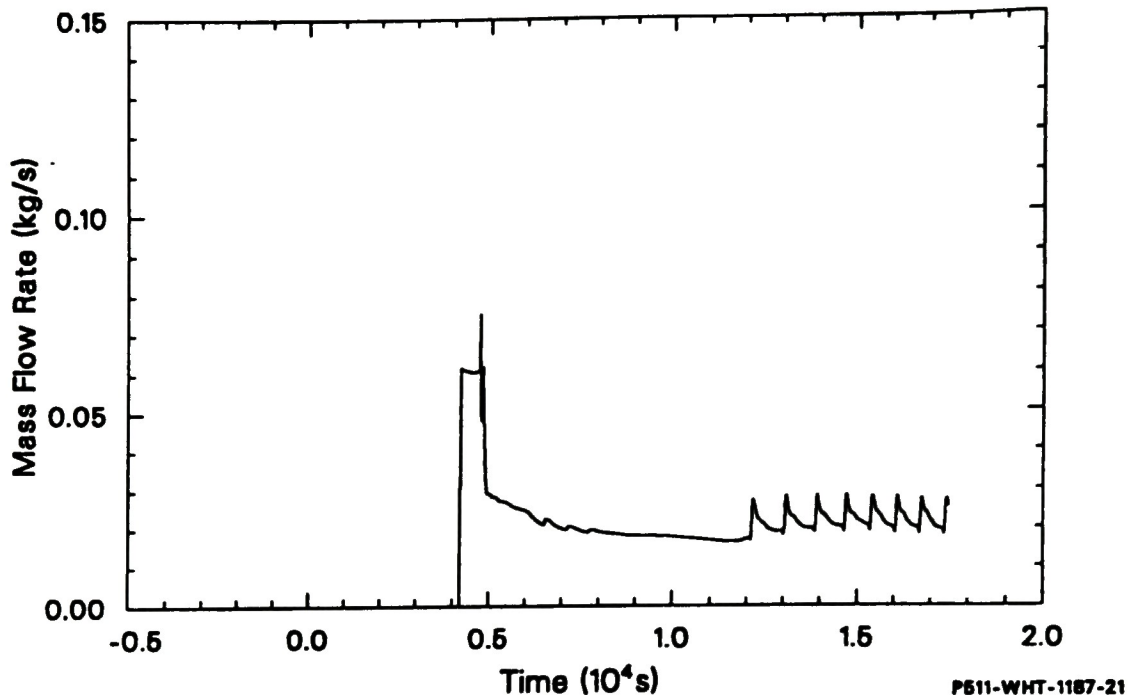


Figure 8. Calculated mass flowrate through PORV by the saturation model with Wilson's correlation.

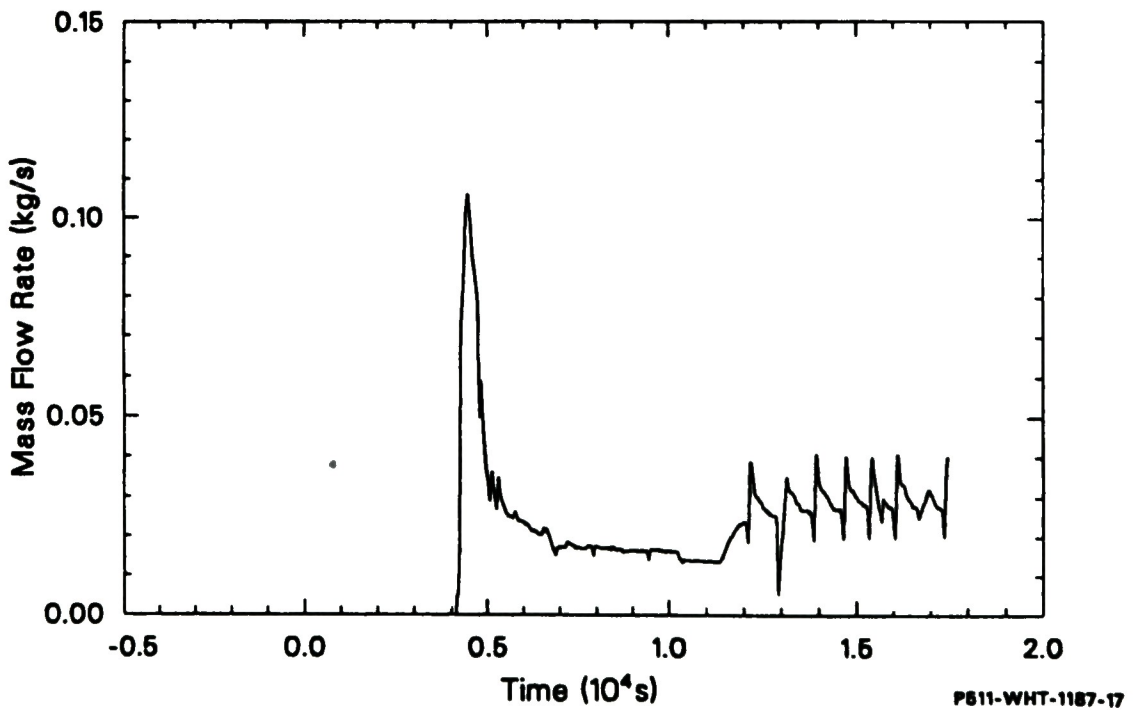


Figure 9. Experimental mass flowrate through the PORV.

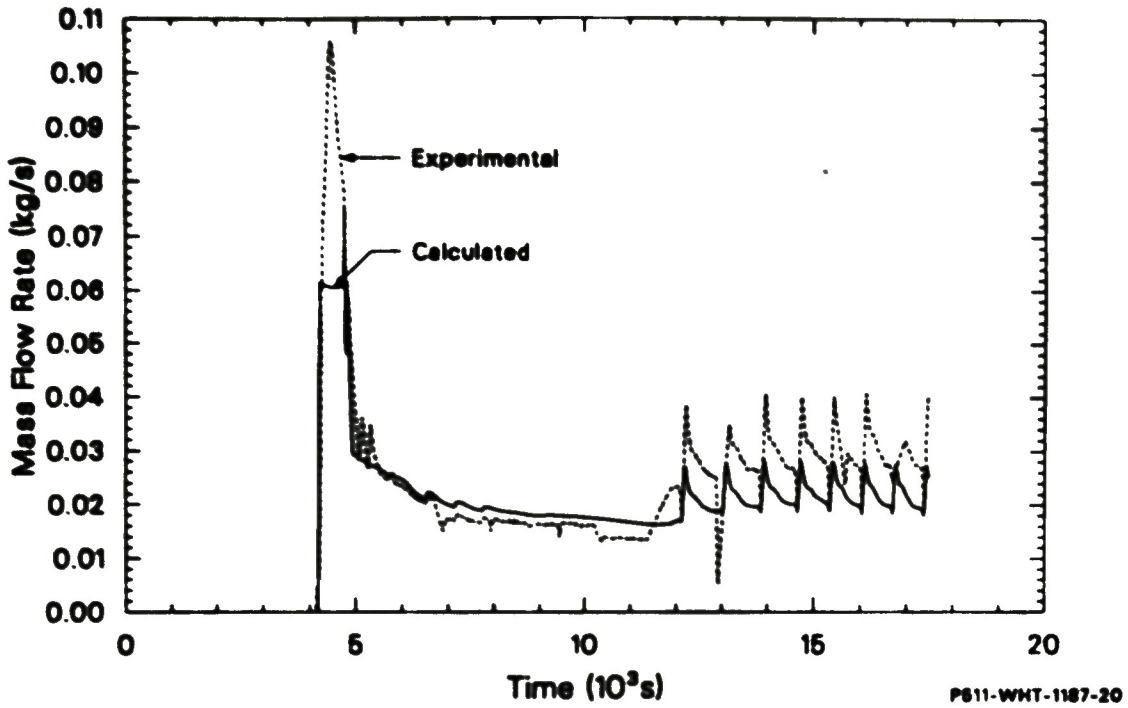


Figure 10. Comparison of calculated results with experimental data (1).

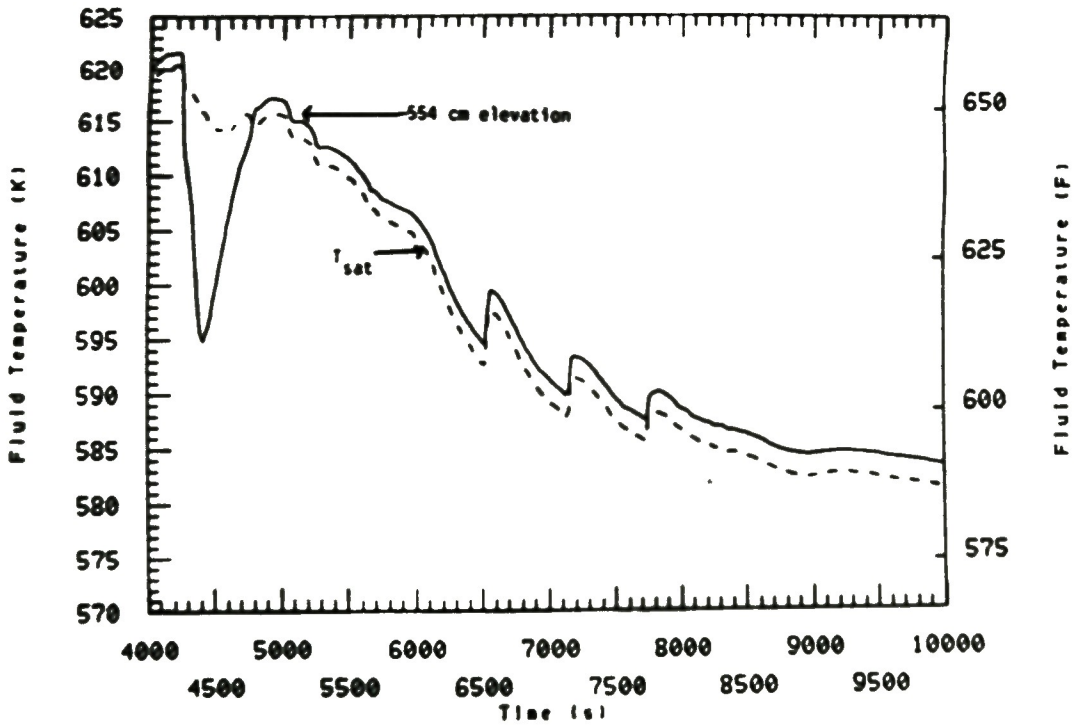
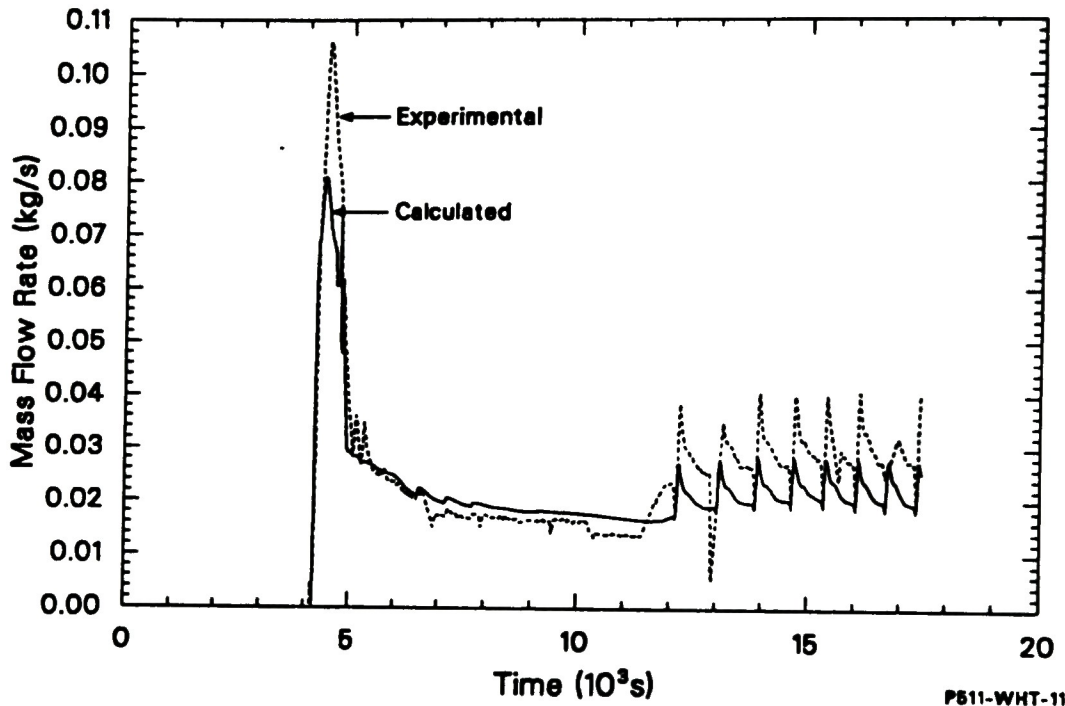


Figure 11. Measured fluid temperature and saturation temperature in the pressurizer.

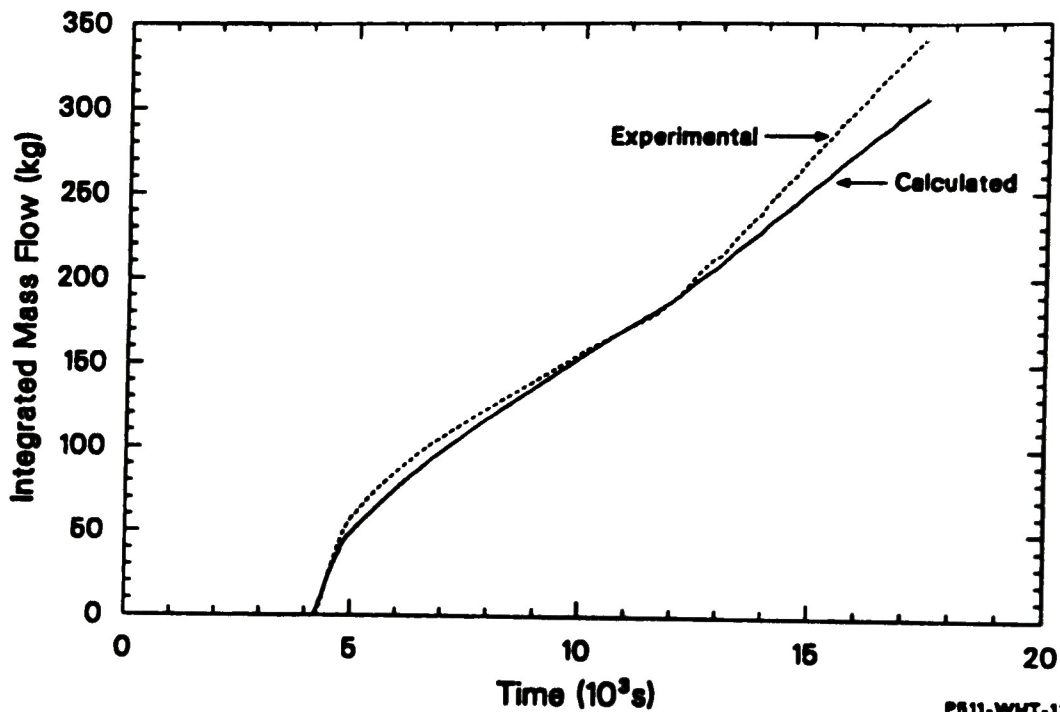


P811-WHT-1187-10

Figure 12. Comparison of calculated results with experimental data (2).

calculation. One of the causes of this difference is that insufficient information is available concerning upstream conditions of the PORV. Part of the discrepancy may also result from the differentiation of the catch tank data to obtain the PORV mass-flowrate (discharge from the PORV was collected in the catch tank and continuously weighed using a load cell, thus providing a measurement of the integrated mass exiting the system through the PORV). Figure 13 compares the subcooled-calculation results for total mass loss with the experimental data. The calculation results in a total mass loss through the PORV which is some 7% lower than the measured mass loss.

Despite some limited disagreement for a period of subcooled flow, the calculation gives generally good results compared with the experiment, and thus is considered to be validation for the PORV mass-flowrate calculational routine. It is considered adequate that modification should be added to the program for subcooled conditions in analysis of the TMI-2 PORV flowrates.



P811-WHT-1187-22

Figure 13. Comparison of calculated results for total mass loss with experimental data.

## 4. CALCULATIONAL CONDITIONS FOR DISCHARGE FLOW

### 4.1 TMI-2 Plant System Configuration<sup>8</sup>

Figure 14 shows the main RCS components. Nuclear fuel in the reactor vessel is cooled by water that circulates into two independent coolant loops, each equipped with a once-through steam generator (OTSG) and two reactor coolant pumps (RCP). The two steam generators are shell-and-tube heat exchangers and are of the once-through type. A unique feature of this Babcock & Wilcox design is that the steam generators are not elevated above the heated core. Therefore, in the event of a loss of pumping power, water in the lower half of the steam generators will be difficult to make available for core cooling if the water level in the system drops below the midplane of the steam generators. The pressurizer can only communicate with the A loop since its surge line comes off from the A loop hot leg. Letdown flow is drawn from the base of the A loop cold leg and is cooled via letdown coolers before flowing into the makeup tank. The high pressure injection (HPI) points are located in all four cold legs on the pump discharge side. There is also provision for two core flood tanks to automatically inject water directly into the core when the system pressure falls below 3.5 MPa (500 psia).

During normal plant operation, the function of the pressurizer is to control system pressure. This is accomplished through the use of pressurizer heaters to increase fluid temperature in the saturated vessel, thus increasing system pressure, and by use of the spray line to inject cold liquid into the vessel, thus reducing temperature and pressure. A cross-sectional diagram of the pressurizer vessel is shown in Figure 15. The PORV is installed on top of the pressurizer to quickly relieve pressure under conditions such as a feedwater pump trip. This is the valve that stuck open and resulted in the TMI-2 accident.

### 4.2 PORV Throat Area and Discharge Coefficient<sup>9</sup>

The PORV used on the top of the pressurizer was manufactured by Dresser Industries with a model number of 31533VX-30. According to the

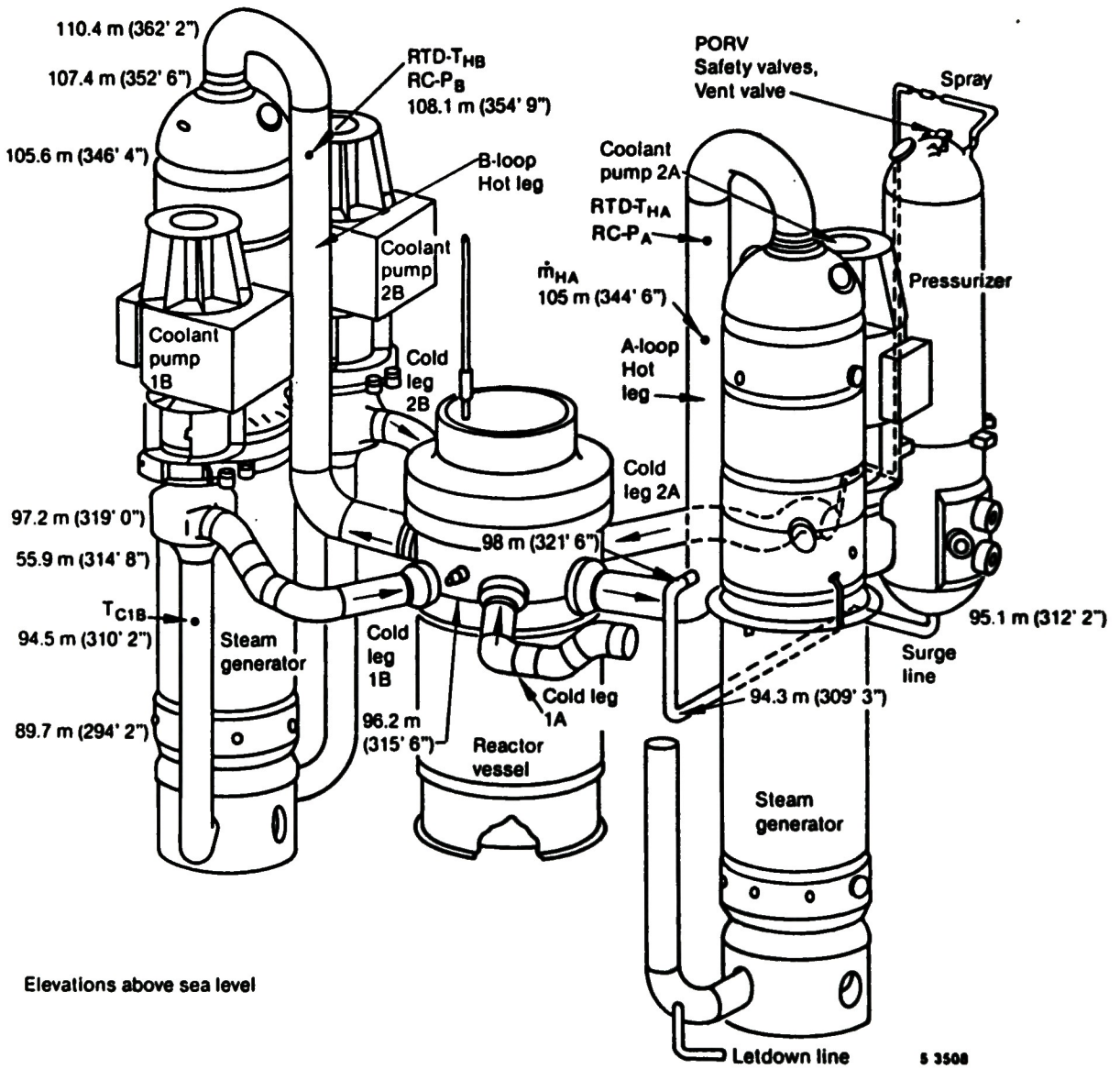
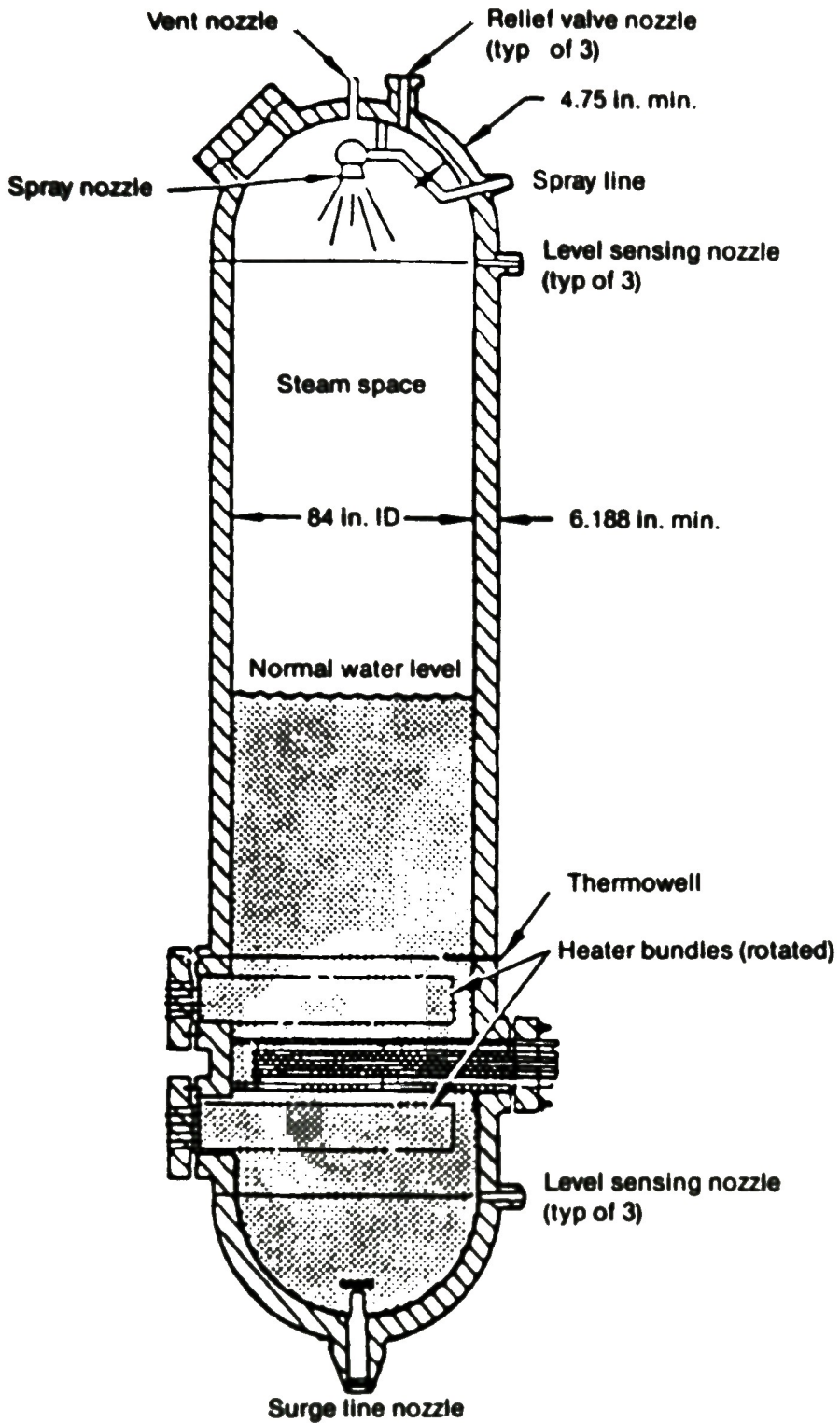


Figure 14. TMI-2 reactor coolant system showing main components.



7-3351

Figure 15. Longitudinal cut-out view of the pressurizer.

report of the EPRI safety and relief valve test program,<sup>10</sup> various Dresser valves with the same model number have different orifice sizes. Six reactors use valves with a 1-3/32 in. orifice, three reactors use valves with a 1-5/32 in. orifice, and eleven reactors use valves with a 1-5/16 in. orifice. The EPRI report identified the TMI-2 PORV as having an orifice size of 1-5/16 in. Although there are several reports describing inconsistent orifice sizes for the valve, the identification made in the EPRI report is considered to be most reliable since this report came out later in time and specifically addressed the relief capacities of valves used in nuclear power plants. The present work assumes an orifice size of 1-5/16 in. for the computation. (NOTE: The TMI-2 PORV valve receiving/inspection report identifies the orifice diameter as 1-5/16 in., and the valve serial number as BN4233. This information was recorded from the valve information plate attached to the valve.)

The PORV in TMI-2 properly opened at its set-point of 15.65 MPa (2270 psig) a few seconds after the initiation of the accident and thereafter remained in the stuck-open position. In the EPRI tests using the same type of valve, all the tested valves opened fully upon actuation. It is assumed in this calculation that the TMI-2 PORV opened fully during the accident. After the PORV opened, whether there was any flow through the PORV depended on the status of the block valve (a 2-1/2-in. motor-operated gate valve) situated upstream of the PORV. Because the block valve flow area was more than twice that of the PORV, when both valves were open the flow out of the pressurizer was limited to the critical flowrate through the PORV.

Table 4 shows the EPRI valve test data together with analysis results. The valve chosen for testing had the Dresser model number 31533VX-30 with an orifice size of 1-5/16 in., the same type as used at TMI-2. Ten valves were tested. Nineteen tests were reported with measured flowrates. These tests were comprised of two steam tests at Marshall Steam Station, and seventeen steam/subcooled-water tests at Wyle Laboratories. Critical mass flux ( $G_{crit}$ ) given in Table 4 was obtained from Davis's critical flow tables. Flow area (Area) is the effective flow area of the orifice computed by dividing measured flowrate by critical mass flux. The

TABLE 4. EPRI DRESSER MODEL 31533VX-30 VALVE FLOW TESTS

Test Number <sup>a</sup>	P (MPa)	T <sub>sat</sub> (K)	T (K)	Flow (kg/s) <sup>b</sup>	G <sub>crit</sub> (kg/m <sup>2</sup> - s) <sup>c</sup>	Area (10 <sup>-4</sup> m <sup>2</sup> )
1	15.82	619.6	619.6	19.54 (s)	24,315	8.04
2	15.89	619.9	619.9	19.54 (s)	24,445	7.99
3	16.23	621.7	626.5	18.27 (s)	24,866	6.94
4	4.34	528.4	462.6	41.72 (l)	73,884	5.65
5	16.75	624.2	514.3	41.34 (l)	75,170	5.50
6	16.07	620.8	538.2	74.36 (l)	133,727	5.56
7	16.27	621.8	503.7	80.79 (l)	150,924	5.35
8	15.98	620.4	620.9	16.79 (s)	24,585	6.90
9	16.70	624.0	617.6	37.21 (l)	71,465	5.21
10	4.77	534.1	507.0	33.12 (l)	57,202	5.79
11	16.00	620.5	508.7	78.49 (l)	147,477	5.32
12	4.56	531.4	320.4	49.00 (l)	98,851	4.96
13	16.62	623.6	616.5	38.11 (l)	72,072	5.29
14	16.27	621.8	608.7	41.74 (l)	77,568	5.38
15	15.83	619.6	615.4	16.33 (s)	24,333	6.70
16	16.55	623.2	607.0	40.84 (l)	80,856	5.05
17	16.48	622.9	609.8	39.02 (l)	77,933	5.00
18	15.72	619.1	613.7	16.70 (s)	24,128	6.92
19	16.55	622.9	608.2	39.93 (l)	29,796	5.00

a. First 2 tests from Marshall steam station, Terrell, NC (Duke Power Co.), others from Wyle Laboratories, Norco, CA.

b. (s) = steam  
(l) = liquid

c. G<sub>crit</sub> from Cliff Davis' program.

effective area for steam flow was determined to be  $(8.02 \pm 0.03) \times 10^{-4} \text{ m}^2$  based on the Marshall steam tests (the first two tests in Table 4), and based on the Wyle Tests, it was  $(6.87 \pm 0.11) \times 10^{-4} \text{ m}^2$ . Because the physical area based on the nominal 1-5/16 in. orifice is  $8.73 \times 10^{-4} \text{ m}^2$ , the discharge coefficient for steam flow is  $0.919 \pm 0.004$  for the Marshall tests and  $0.787 \pm 0.013$  for the Wyle tests. The discharge coefficient for subcooled flow is deduced from the Wyle tests to be  $0.60 \pm 0.03$ . In the present work, discharge coefficients of 0.787 for steam and two-phase flow, and 0.60 for subcooled flow (upstream stagnation condition) are assumed in the calculation.

#### 4.3 Operation of PORV and Thermal Hydraulic Transient<sup>11,12</sup>

The loss of fluid from the RCS was the key factor leading to severity of the TMI-2 accident. The accident was initiated by a loss of normal feedwater to the steam generators resulting in a turbine trip. Between 2 and 6 s after the turbine trip, the RCS pressure reached the PORV set-point of 15.7 MPa (2275 psia) but continued to rise despite opening of the PORV. The reactor shut down automatically due to a high-pressure signal exceeding the set point for scram, as expected. Within a few seconds the RCS pressure dropped to normal values. The PORV, which relieved excess pressure as intended, should have closed when pressure was reduced sufficiently. Instead, it failed and caused a further decrease in system pressure. Figure 16 shows the RCS pressure and the pressurizer level as a function of time during the accident.

The pressurizer level showed an initial drop from the half-full position but quickly turned around and rose sharply to off-scale high (greater than 1016 cm or 400 in.). The pressurizer level indication returned on scale after 10 min into the accident but remained high, ranging from 914 to 990 cm until 94 min. At this time, the auxiliary feed water (AFW) was increased to the A-loop steam generator (SG) resulting in a short RCS depressurization, and a drop in the pressurizer level. During the first 100 min, continued system depressurization, due to flow out of the open PORV, resulted in an increasingly voided RCS. The RCS fluid

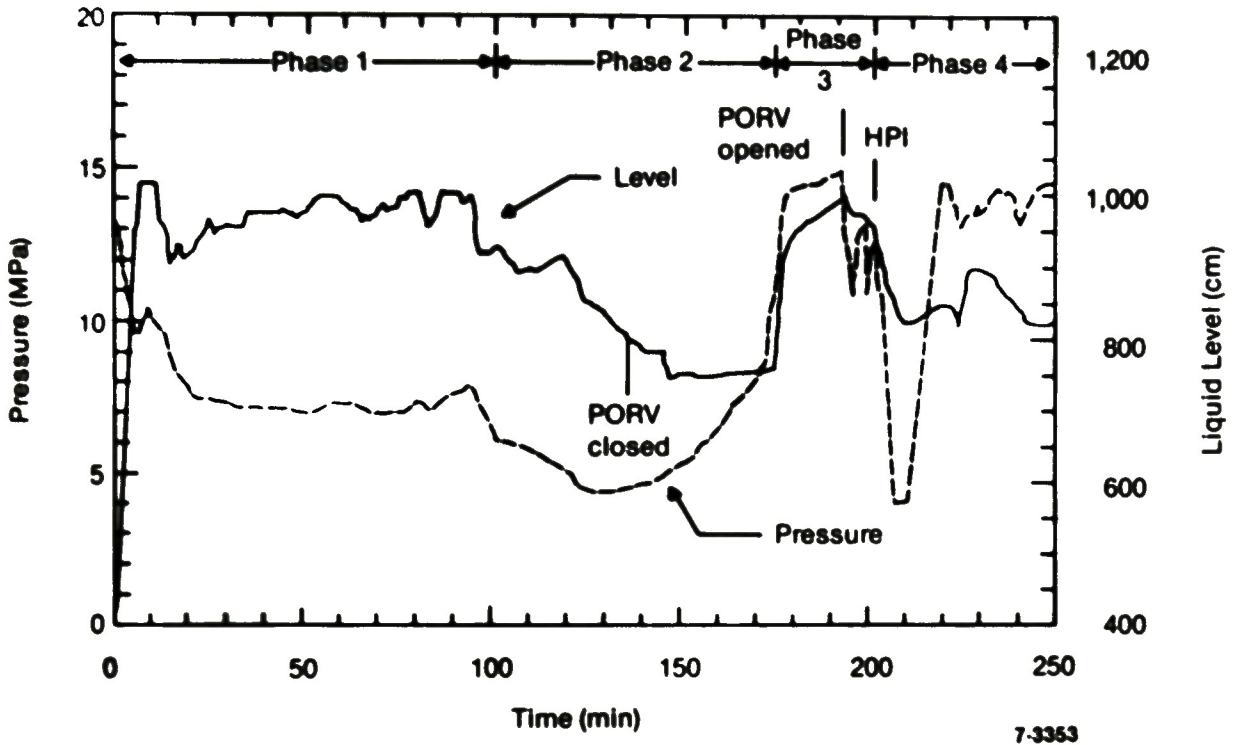


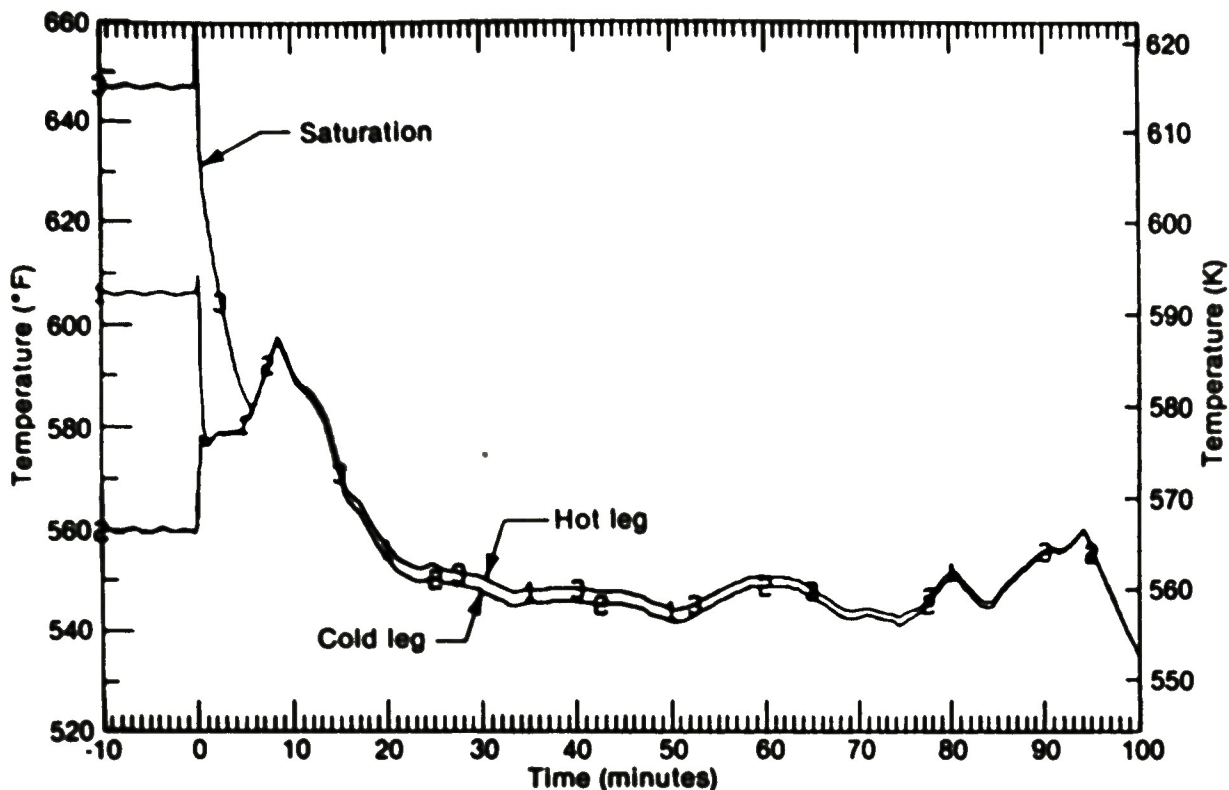
Figure 16. Pressurizer level and primary system pressure.

temperatures were nearly equal to the saturation temperature as indicated in Figure 17. The flow throughout the RCS was, therefore, homogeneous two-phase flow.

As a result of increased feedwater to the A-loop OTSG at 94 min, the steam condensation rate increased, causing pressure in the RCS to drop sharply. This abrupt drop in pressure and temperature resulted in a drop in the pressurizer level as the previously saturated liquid in the pressurizer flashed into steam. Backflow out of the pressurizer might also have occurred, resulting in a decrease of the level.

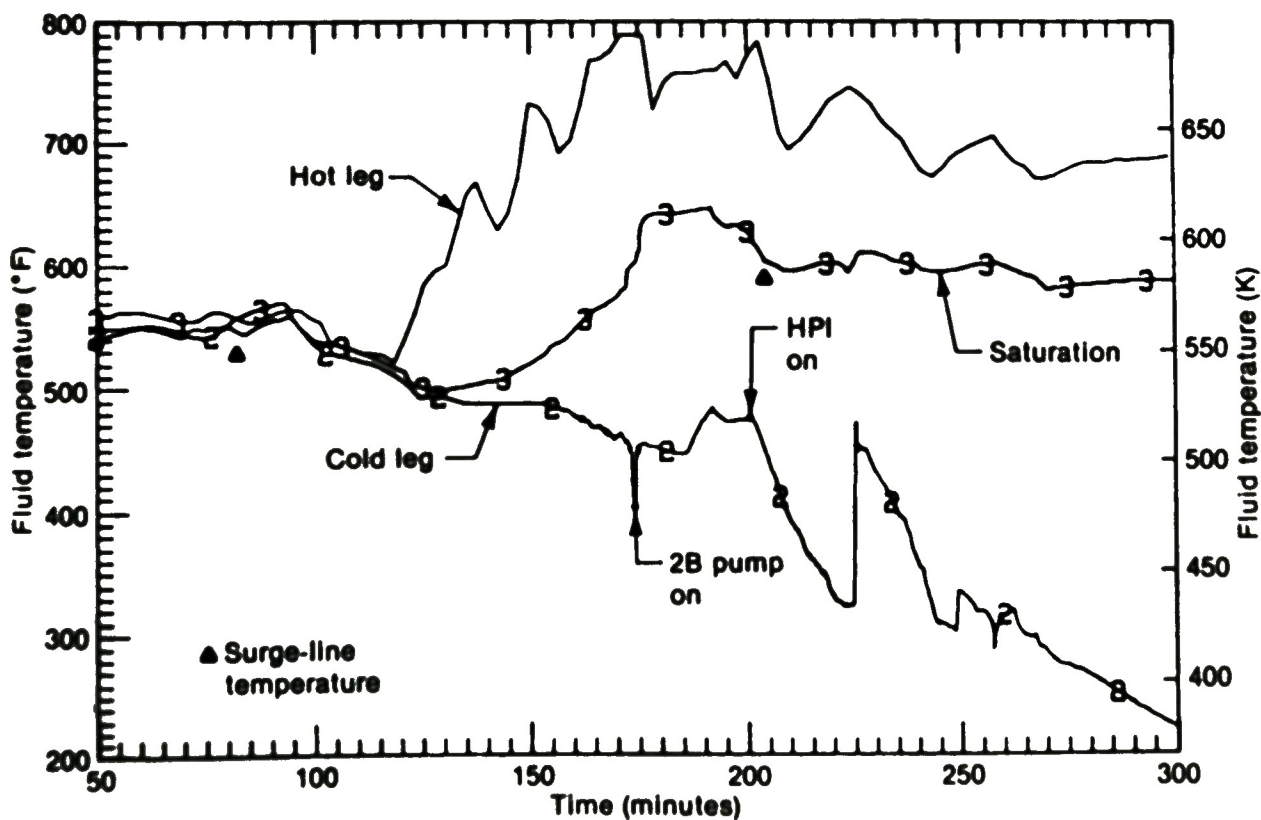
At 100 min, both A-loop pumps were stopped (the B-loop pumps had been stopped at 73 min), and the previously homogeneous two-phase mixture in the RCS stratified with a level in the vicinity of the top of the core (below the surge-line elevation in the hot leg). Starting at this time, the liquid pool in the core was boiling, sending steam flow into the pressurizer surge-line and out of the PORV. Until the PORV block valve was closed by an operator at 139 min, steam velocities were high enough into the surge line that backflow from the pressurizer was limited by counter-current flow interference. The pressurizer liquid level continued to decrease due to steam generation by the pressurizer heaters and thus saturation conditions were maintained in the pressurizer.

At 174 min, the RCP-B pump was briefly restarted, and the pressurizer level abruptly increased due to a large in-surge resulting from the abrupt increase in RCS pressure. The pressurizer drain at 200 min was a result of RCS depressurization induced by steam condensation due to the cold HPI injection liquid in the cold legs and the core. Refill of the pressurizer at 210 min was a result of the continuation of HPI injection into the RCS enough to cover the surge line entrance. The PORV block valve was opened at 220 min, resulting in the pressurizer level returning on scale. Surge-line temperature was recorded at 206 min to be 578 K (581°F) as indicated in Figure 18. The PORV block valve was operated several times to control the primary system pressure during this time period.



6 0643

Figure 17. A-loop hot leg, cold leg, and saturation temperatures (1).



6 0645

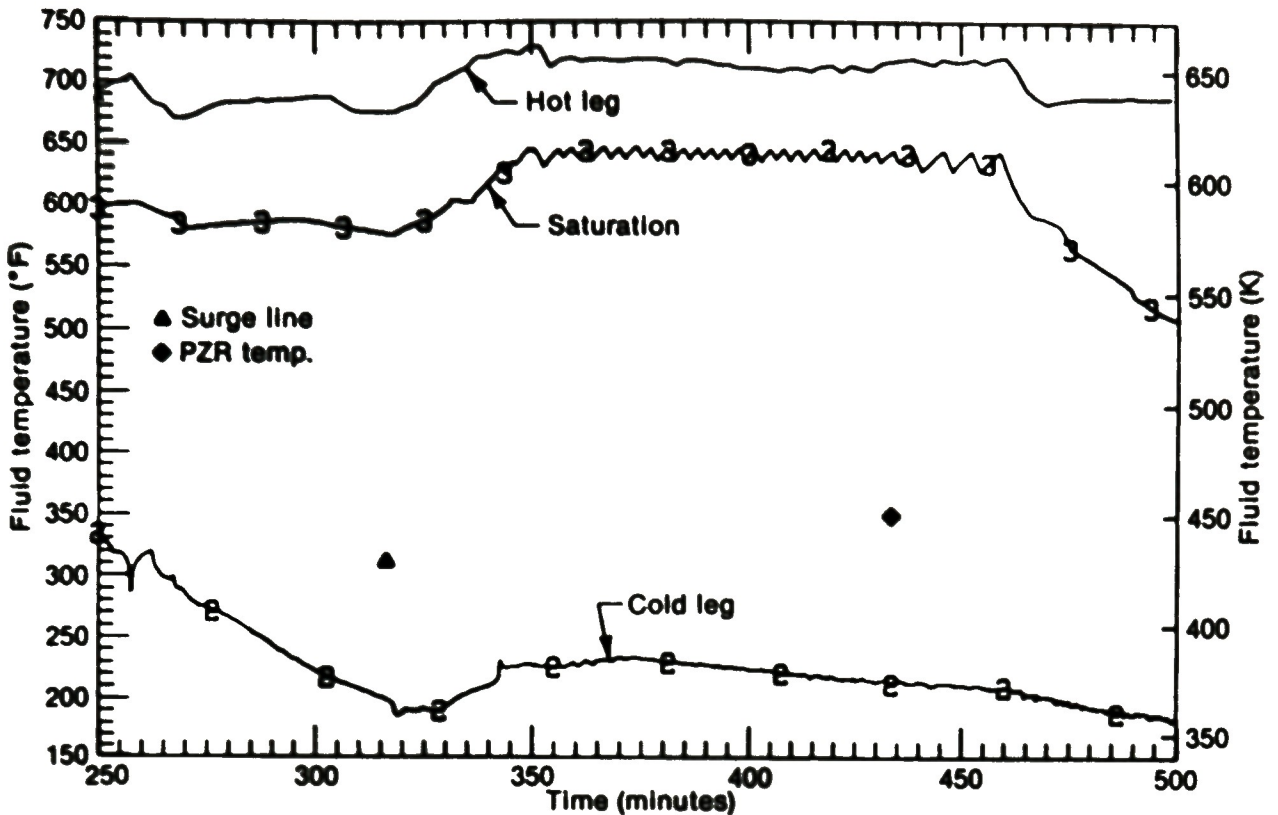
Figure 18. A-loop hot leg, cold leg, and saturation temperatures (2).

At 225 min, the A-loop cold-leg temperature jumped by 70 K (130°F), probably due to reverse flow into the A-loop cold leg. This is believed to have been caused by molten fuel falling into the liquid pool in the lower plenum, forcing the hot liquid in the downcomer back into the cold legs.

Sustained HPI liquid injection into the primary system began at 267 min. Consequently, the primary system temperature decreased and the pressurizer surge-line temperature was recorded at 315 min as 424 K (303°F) as shown in Figure 19. The pressurizer level briefly increased to off-scale high due to sustained HPI injection and flow out of the PORV at 270 min. Saturation condition was probably maintained in the pressurizer during this time since sufficient heat was supplied by the pressurizer heaters, and RCS pressure was still low.

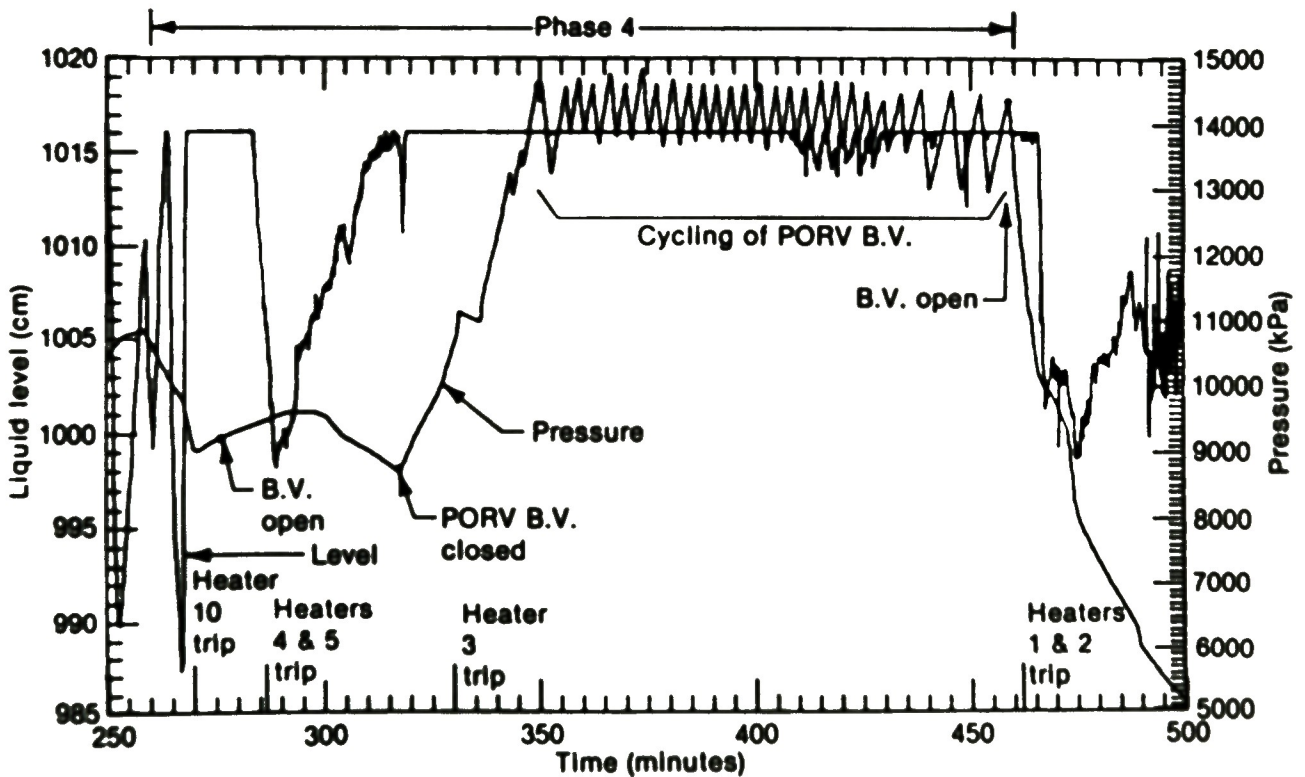
The pressurizer level increased to off-scale (high) again at 315 min, but this time the off-scale level was sustained and reduced heat input by the active pressurizer heaters suggests the initiation of subcooling in the pressurizer. At 318 min, the PORV block valve was closed to repressurize the primary system. With the block valve closed and continued makeup, the RCS pressure increased from 8.7 to 14.7 MPa (1260 to 2130 psig) in 30 min. From this time to 454 min, the PORV block valve was cycled open and closed to maintain the RCS pressure between 13.1 to 14.5 MPa (1900 to 2100 psig) as shown in Figure 20. During the periods when the PORV block valve was open, flow out of the PORV was considered to be all liquid since the pressurizer level was measured to be off-scale full and the pressurizer temperature was recorded at 433 min at 445 K (342°F), some 170 K below the saturation temperature.

At 459 min, when the PORV block valve was opened, a rapid sustained depressurization of the RCS was initiated as shown in Figure 21. The pressure measurement indicates 3 MPa (435 psig) at 554 min when the PORV block valve was closed for a short time. This depressurization, together with temperature rise by the heaters, caused the pressurizer temperature to close to the saturation temperature, and at 625 min they were essentially equal, as shown in Figure 22.



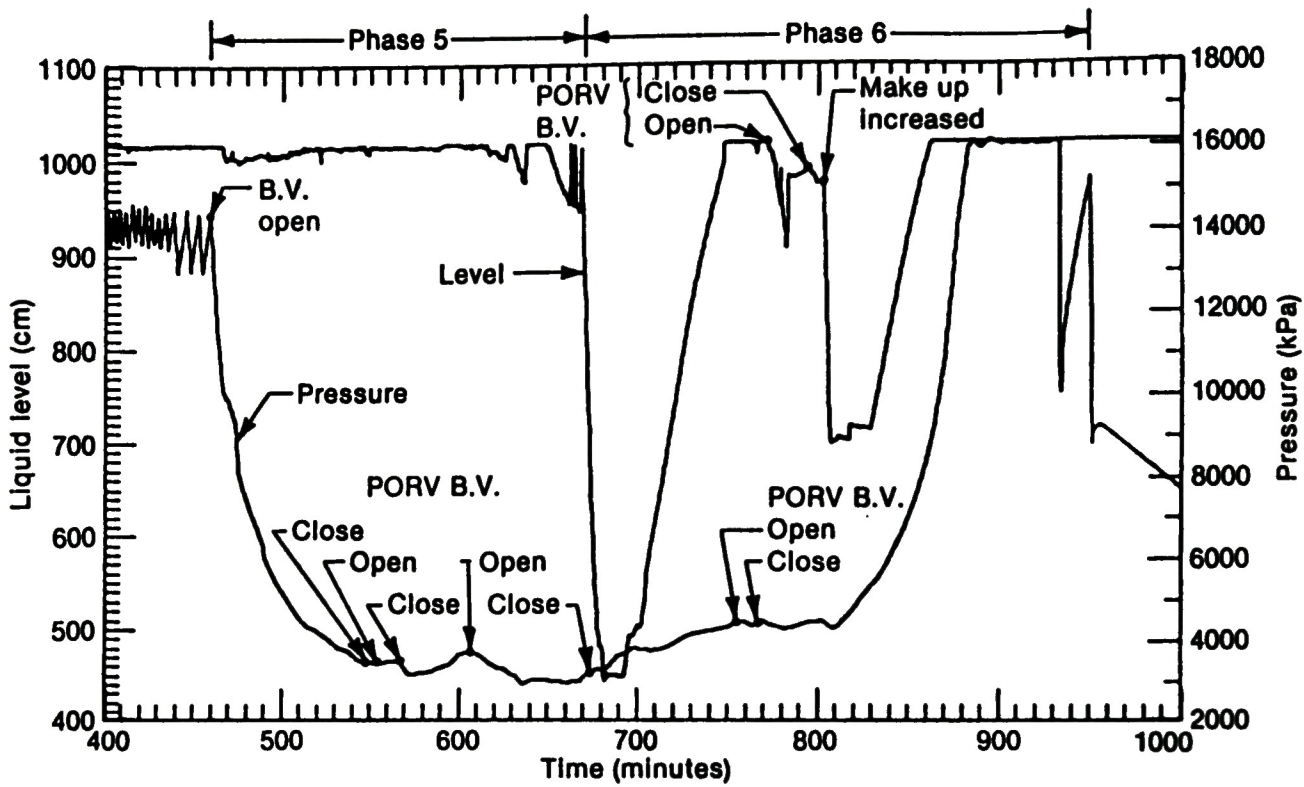
8 0647

Figure 19. A-loop hot leg, cold leg, and saturation temperatures (3).



8 0648

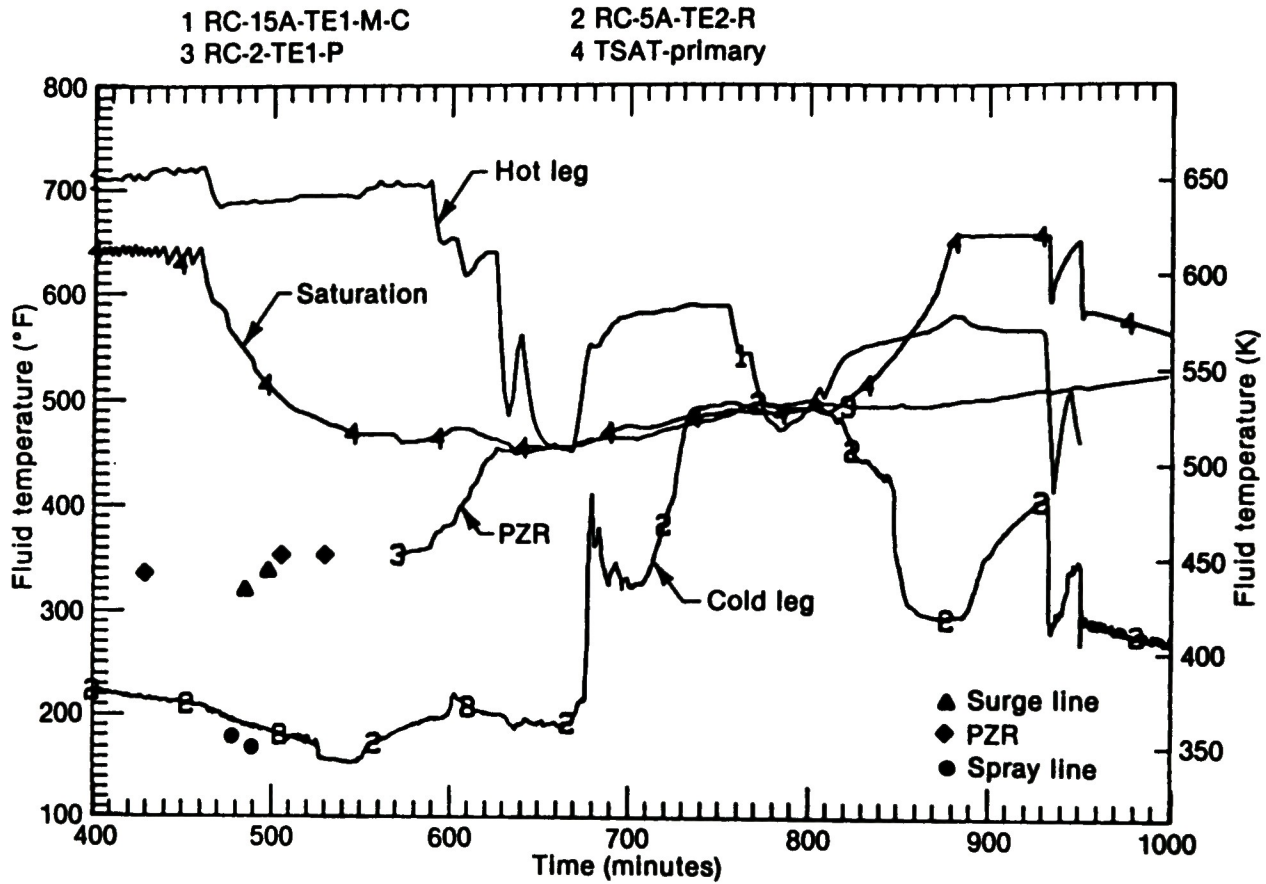
Figure 20. Comparison of pressurizer liquid level and primary system pressure (1).



6 0848

Figure 21. Comparison of pressurizer liquid level and primary system pressure (2).

The PORV block valve was closed for the rest of the accident at 795 min and repressurization and recovery of the primary system initiated from this time. Table 5 shows the entire operation sequence of the PORV block valve during the TMI-2 accident.



6 0849

Figure 22. Comparison of system temperatures (A-loop hot and cold and PZR) with saturation.

TABLE 5. PORV BLOCK VALVE OPENING AND CLOSING TIMES

<u>Opening Time</u> (min)	<u>Closing Time</u> (min)	<u>Interval</u> (min)
.0	139.0	139.0
191.6	194.8	3.2
197.9	198.4	0.5
220.0	318.0	98.0
343.0	343.6	.6
345.5	346.0	.4
349.3	349.8	.5
350.5	352.5	2.0
356.0	357.0	1.0
359.1	360.4	1.3
362.3	363.8	1.4
366.5	376.9	1.4
370.0	371.4	1.4
374.0	375.5	1.4
377.3	378.7	1.4
381.1	382.5	1.5
384.7	385.9	1.2
387.9	389.2	1.3
391.1	392.3	1.3
394.4	395.6	1.2
397.7	398.9	1.3
401.1	402.7	1.6
405.0	406.2	1.2
408.2	409.6	1.4
411.7	413.1	1.4
415.5	416.9	1.4
418.9	420.3	1.5
422.5	424.1	1.5
426.1	427.1	1.0
429.9	430.6	.7
434.0	435.0	1.0
438.7	440.4	1.7
445.8	447.6	1.8
452.5	454.3	1.8
459.0	554.4	95.4
560.5	570.0	9.5
589.0	589.1	.1
601.0	672.0	71.0
754.5	763.0	8.5
772.0	795.0	23.0



## 5. CALCULATIONAL RESULTS AND ASSESSMENT

In this chapter, comparisons of calculated results between the saturation and the subcooled models, and Wallis's and Wilson's equations are presented. Subsequently, a maximum flow limiting case and a best-estimate case are considered to estimate the mass flows through the PORV during the accident.

### 5.1 Comparison of Saturation Model and Subcooled Model

Figure 23 shows calculated mass-flowrates through the PORV as a function of time from 0 to 390 min by the saturation model with Wallis's equation. It is seen from this figure that the PORV block valve was cycled open/close three times after shut-off at 139 min into the accident, and the average discharge flowrate during open time of the valve is approximately 19 kg/s. As described in the previous chapter, the pressurizer surge-line temperature was recorded on a utility printer at 206 min to be 581°F, which is nearly equal to the saturation temperature. Between 206 min and 315 min, there was no record of the fluid temperature in the vicinity of the pressurizer. The record of the surge-line temperature at 315 min was 303°F, some 300°F below the saturation temperature. Here a maximum flow limiting case is considered, in which a linear decrease in fluid enthalpy with time from 206 min to 315 min is assumed. Calculated mass-flowrates for this subcooled model are plotted in Figure 24, and the average discharge flowrate is computed to be about 31 kg/s, some 1.5 times over the average value for the saturation model. Figure 25 compares the integrated mass-flows of the two calculation models during the initial 320 min. Differences of integrated mass-flows becomes  $\sim 2 \times 10^5$  kg at the end of this time. Notice that the difference becomes obvious from 206 min when the pressurizer fluid begins to be subcooled.

### 5.2 Comparison of Wallis's and Wilson's Equation

Figures 26 and 27 show the difference between two calculational cases; one is by Wilson's equation [Eq. (5)] and the other is by Wallis's equation [Eq. (4)] for the steam velocity calculation. As shown in the void

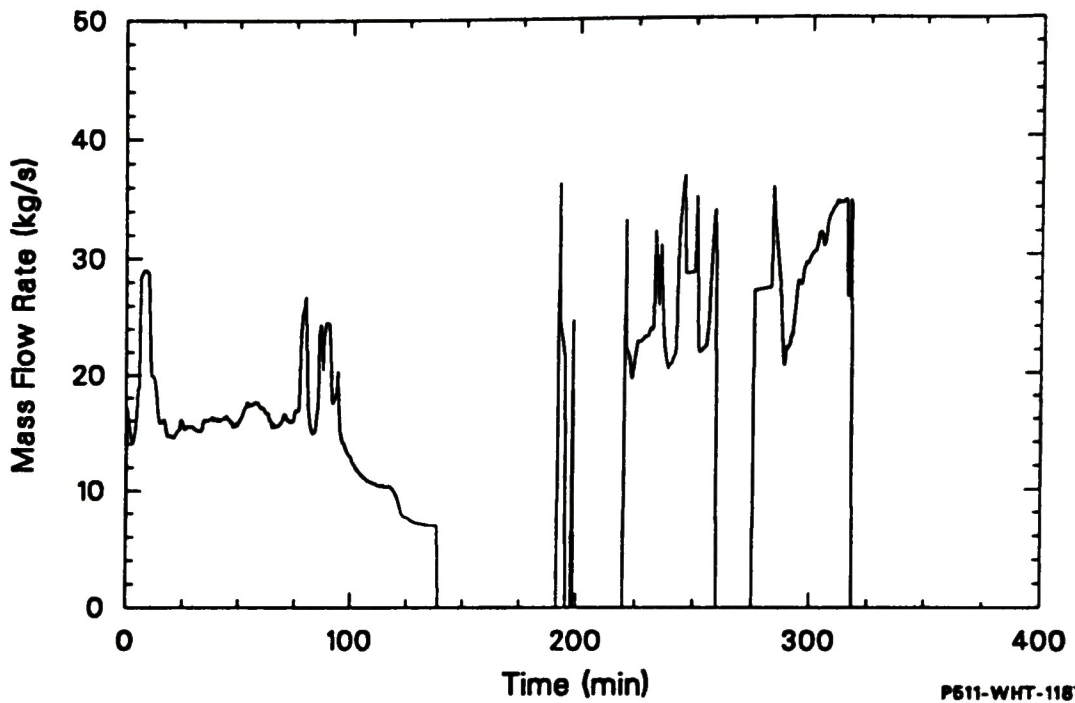


Figure 23. Calculated mass flowrate through PORV by the saturation model.

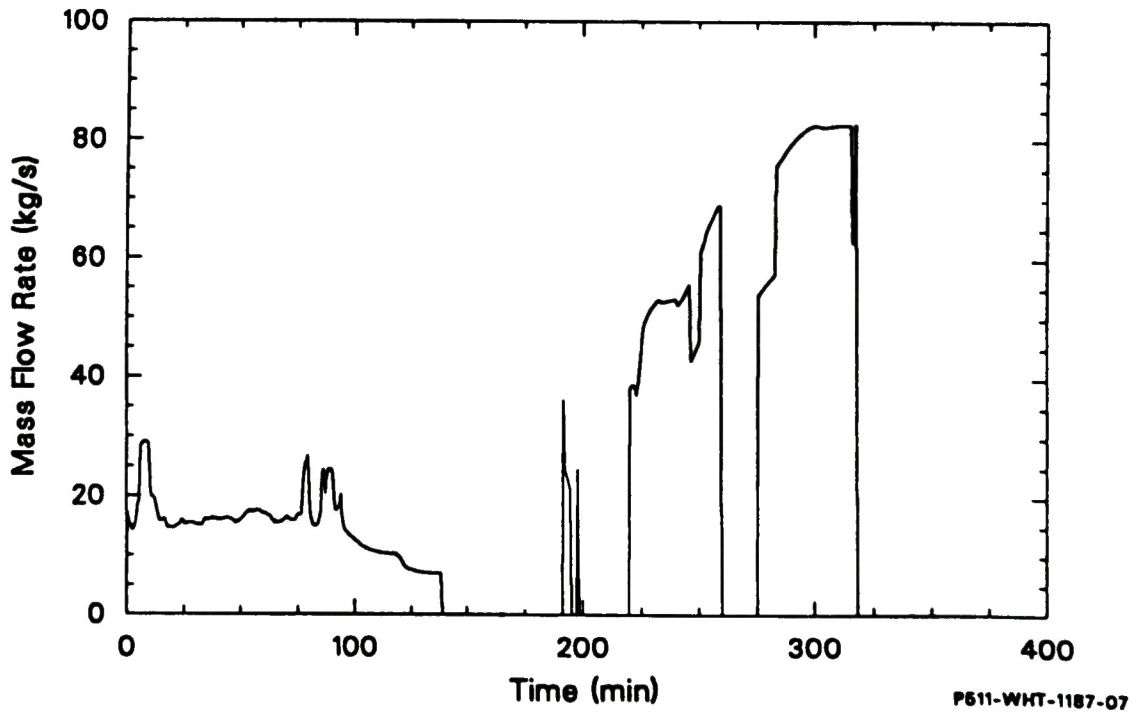
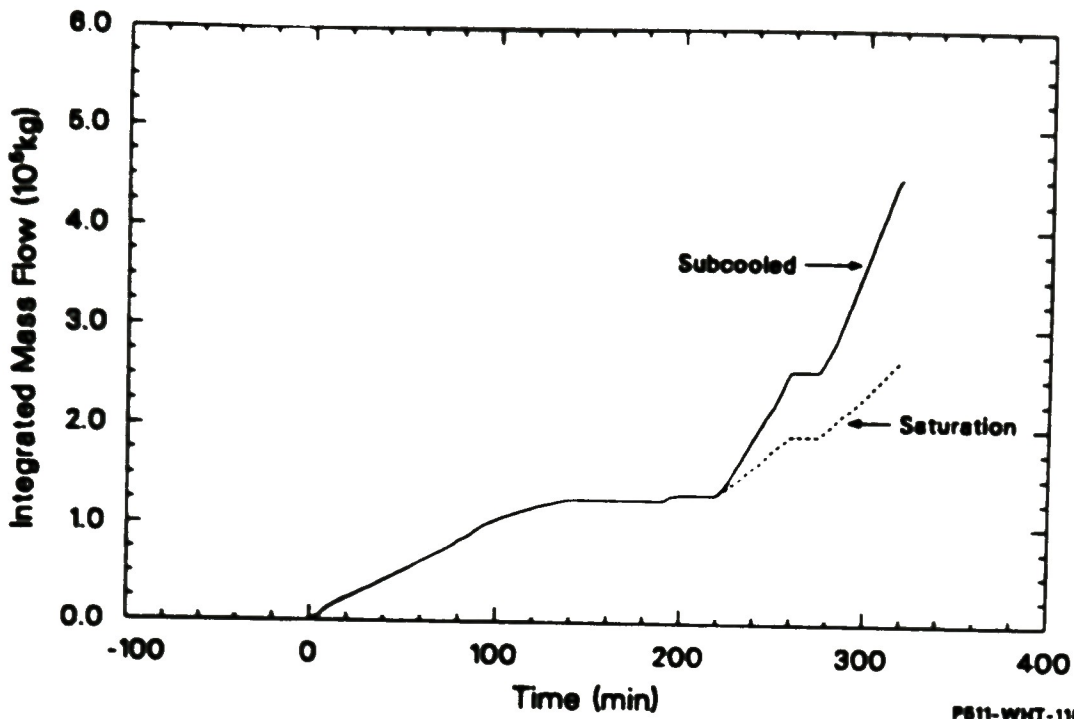
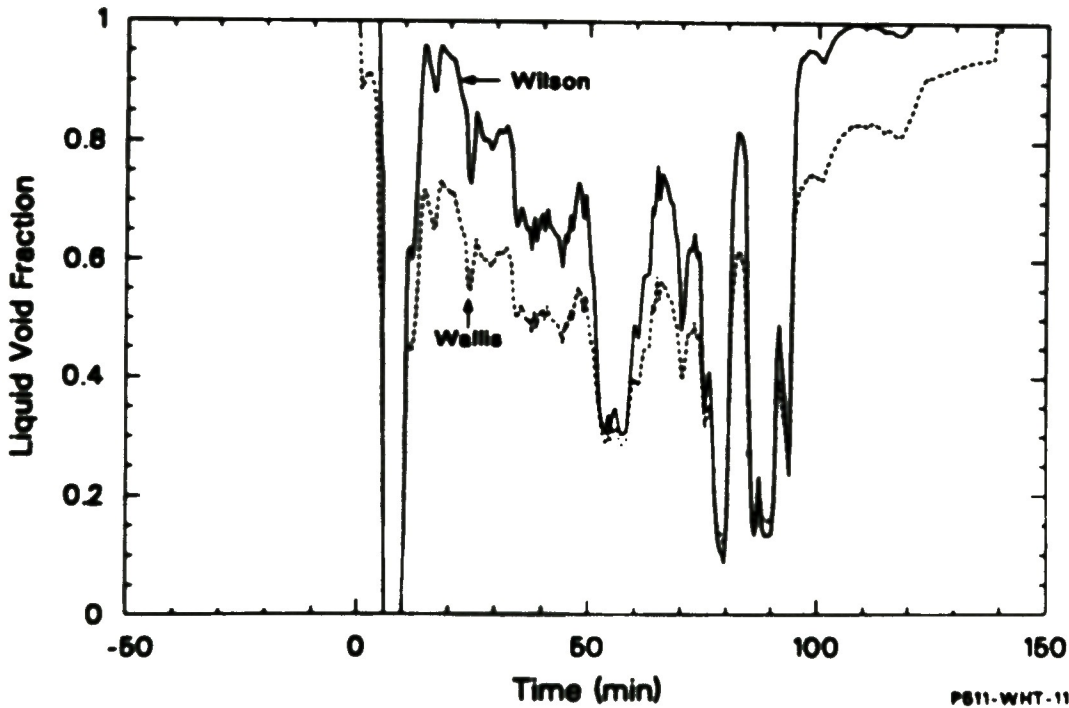


Figure 24. Calculated mass flowrate through PORV by the subcooled model.



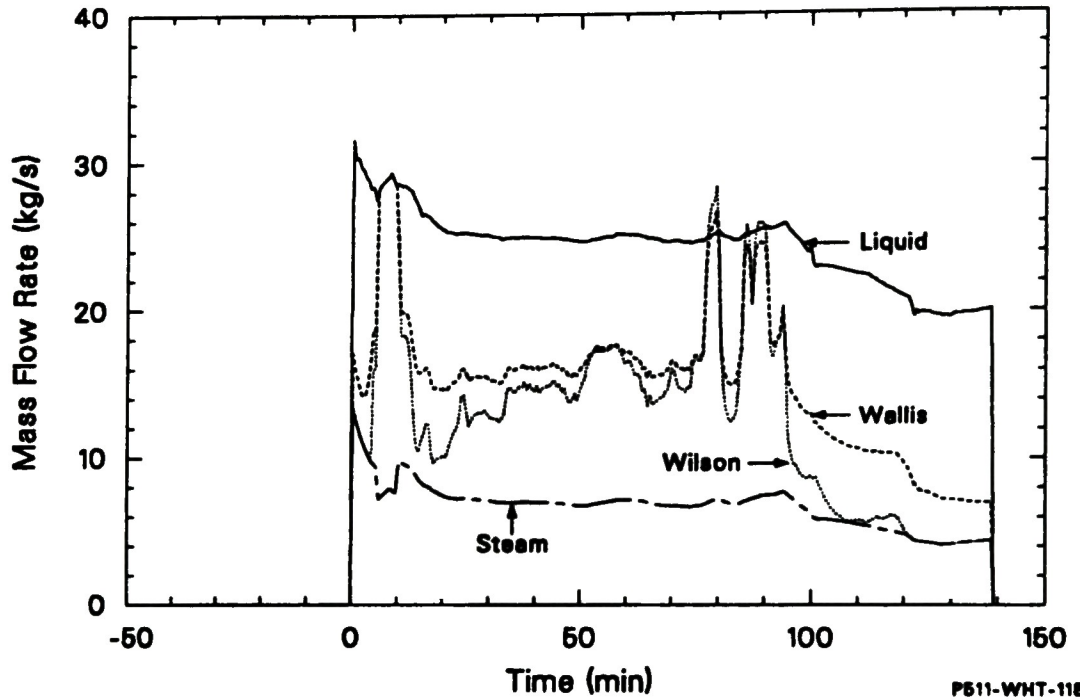
PS11-WHT-1187-18

Figure 25. Comparison between integrated mass-flows by the saturation and subcooled models.



PS11-WHT-1187-02

Figure 26. Calculated PORV void-fractions by Wilson's and Wallis's correlations.



PS11-WHT-1187-01

Figure 27. Comparison of calculated mass flowrates for all-steam, all-liquid, and two-phase flow by Wilson's and Wallis's equations.

fraction plot of Figure 26, Wallis's equation underestimates steam flows as compared to Wilson's equation. The Wilson correlation was developed from experimental data obtained under conditions very similar to the TMI case being considered, and is believed to produce more reasonable results. A case in point is the period after 100 min, with the RCPs off and no forced flow through the loops. Independent analysis indicated that the hot-leg coolant level was below the surge-line entrance. Thus, only steam was flowing into the pressurizer, and flow out of the PORV would have quickly equilibrated to nearly all steam flow. Comparison of the calculational results by the Wilson and Wallis models shows that the Wallis model results in mass-flowrates much larger than the all-steam flowrates, whereas the Wilson model results in near steam flowrates as shown in Figure 27. Difference of integrated mass-flow becomes  $\sim 2 \times 10^4$  kg at 300 min as shown in Figure 28. As a result of these considerations, the Wilson model is considered to be superior for the TMI-2 Accident simulation, and is used in the best-estimate calculation.

### 5.3 A Maximum Flow Limiting Case

In the following, an extension of the limiting case described in Section 5.1 is considered, in which a linear increase in fluid enthalpy with time from 315 min to 570 min is assumed, then the measured pressurizer-temperatures are used at every 2 min to obtain the effluent fluid enthalpy from 570 min to 625 min. Further, from 625 min, saturation conditions are assumed for the pressurizer fluid. Figures 29 and 30 show calculated mass-flowrates from 0 to 600 min by Wilson's equation and by Wallis's equation, respectively, for this limiting case. From 206 min to 625 min, the effluent fluid was assumed to be subcooled liquid without steam so that there can be no difference between mass-flowrates calculated by the two models. The fine structure observed in these figures from 350 min to 454 min corresponds to the open/close cycling operation of the PORV. After 625 min, discharge flow is a two-phase mixture with low quality; thus, there can be small difference between mass-flowrates by the two models. In terms of integrated mass-flow through the PORV, Wallis's equation gives some  $2 \times 10^4$  kg larger difference than Wilson's at the last PORV closure time of 795 min as shown in Figure 31.

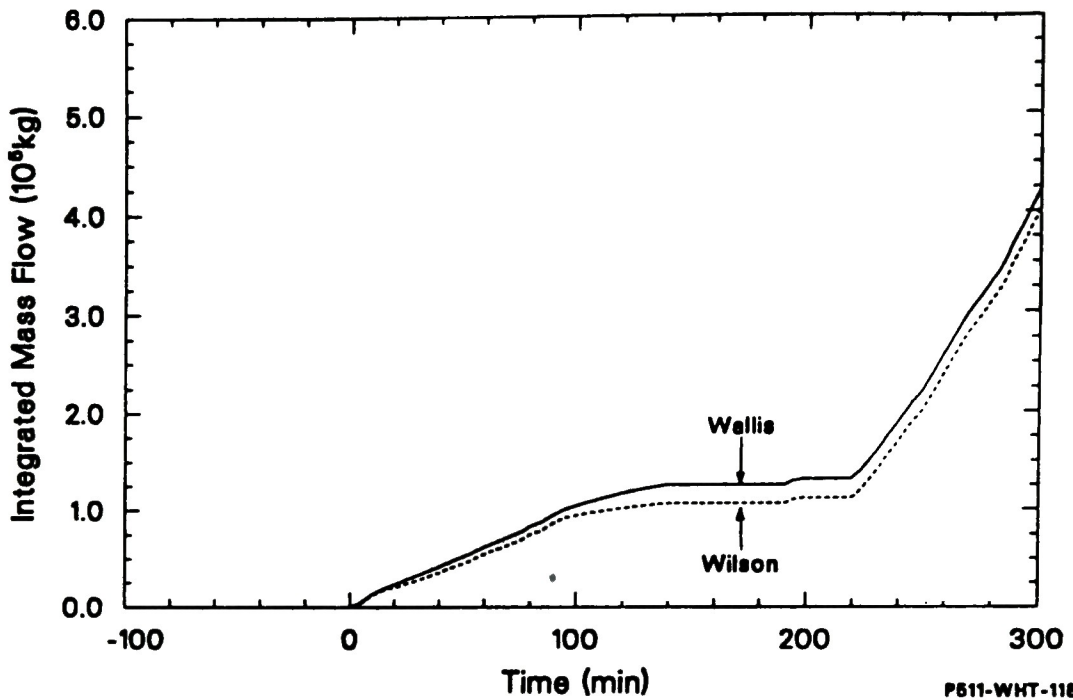


Figure 28. Comparison of integrated mass-flow calculated by Wilson's and Wallis's equations.

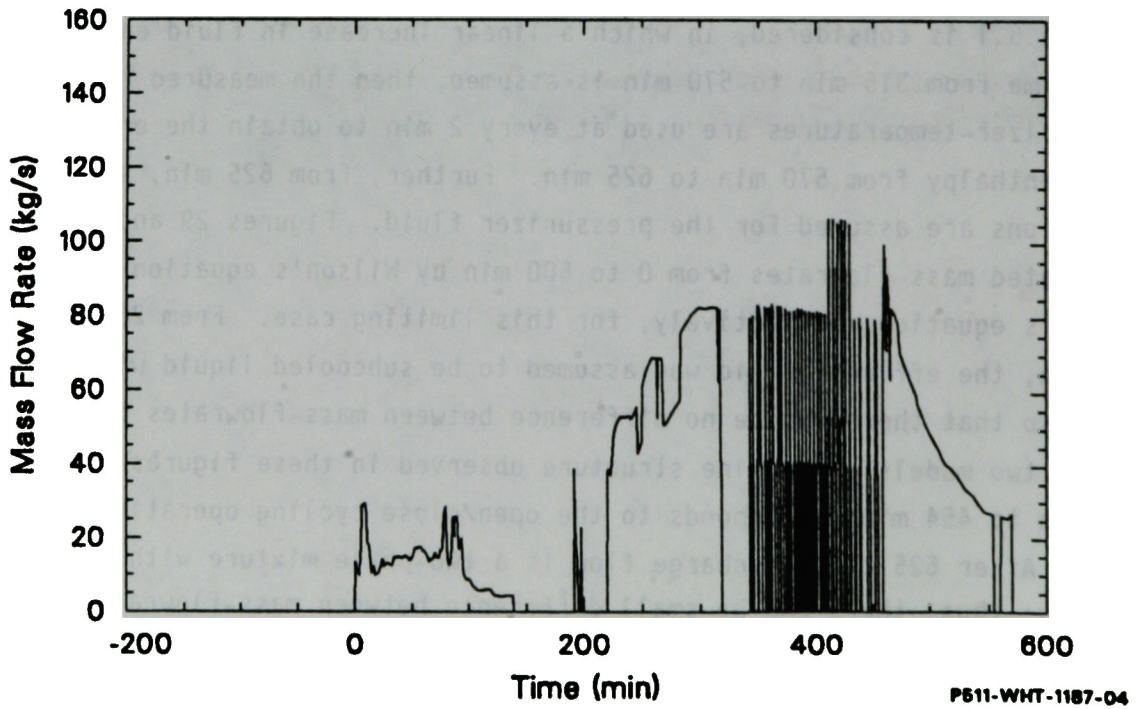


Figure 29. Calculated mass flowrate by Wilson's equation.

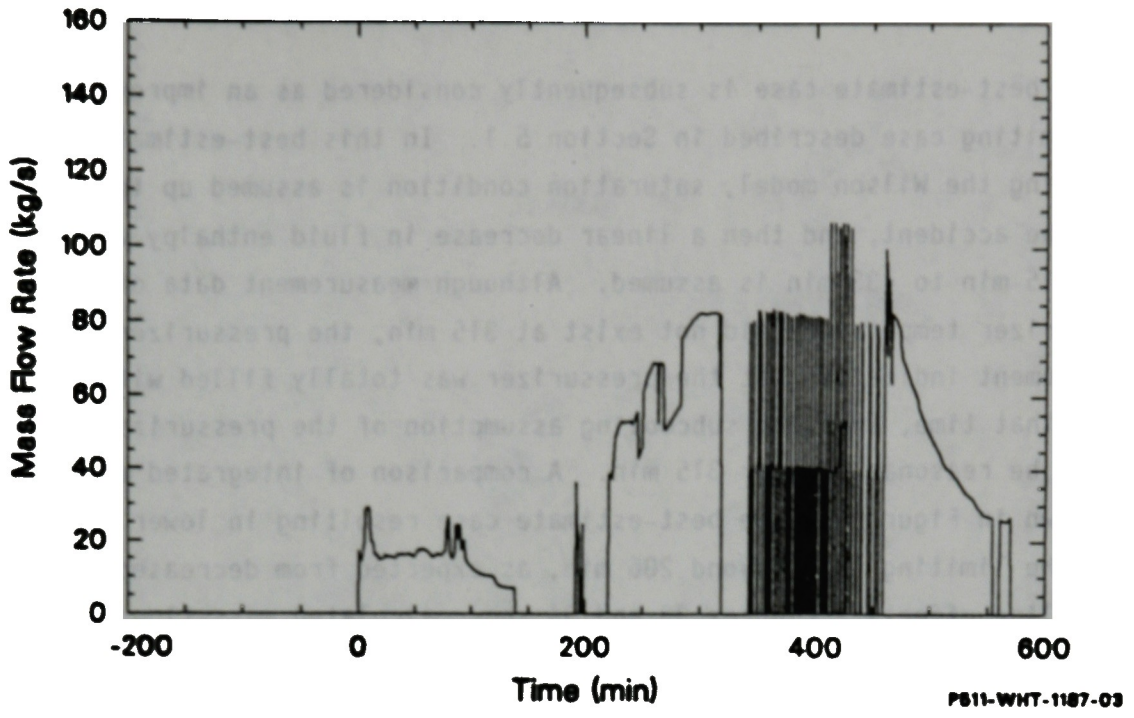


Figure 30. Calculated mass flowrate by Wallis's equation.

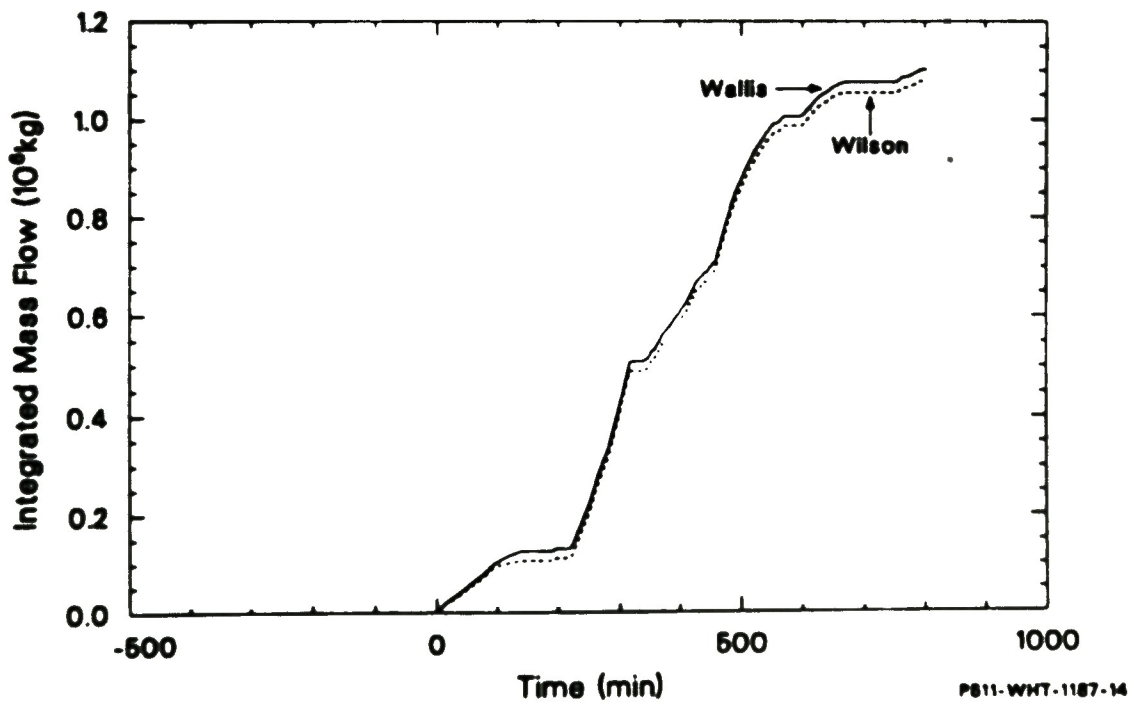
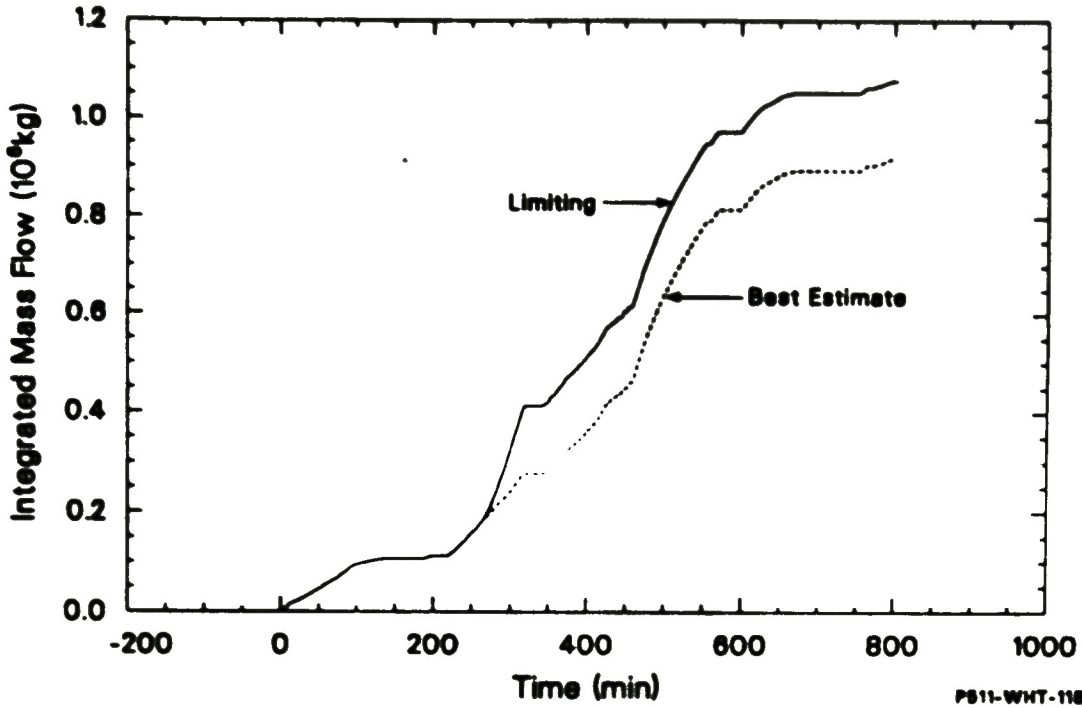


Figure 31. Comparison of integrated mass-flow calculated by Wilson's and Wallis's equations.

#### 5.4 A Best-Estimate Case

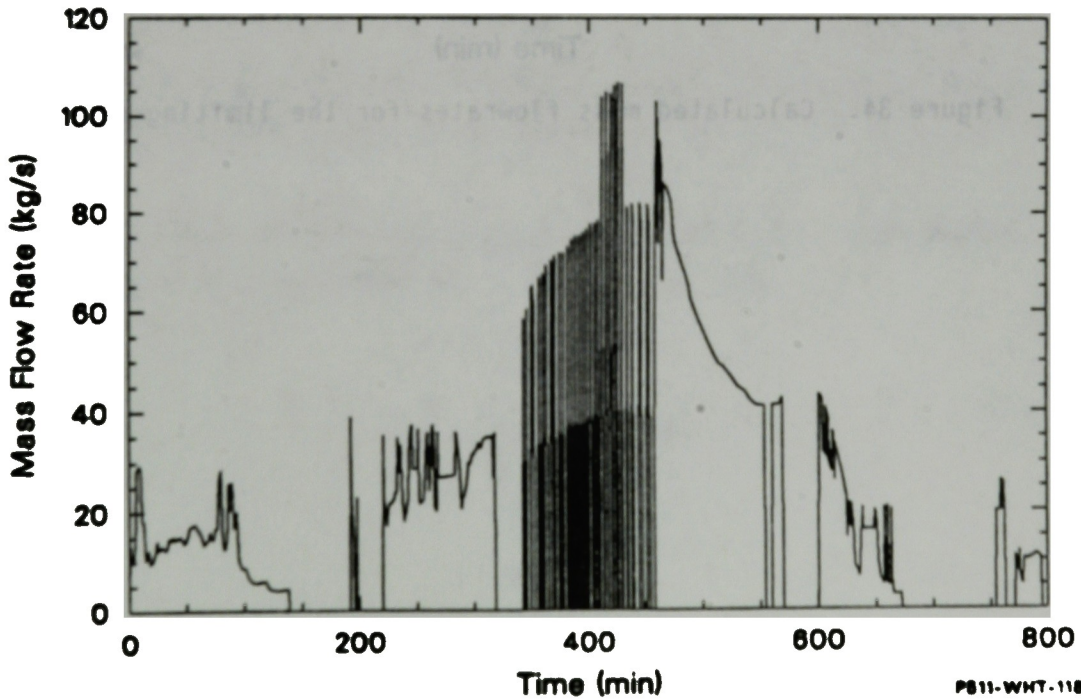
A best-estimate case is subsequently considered as an improvement on the limiting case described in Section 5.1. In this best-estimate case, employing the Wilson model, saturation condition is assumed up to 315 min into the accident, and then a linear decrease in fluid enthalpy with time from 315 min to 433 min is assumed. Although measurement data of the pressurizer temperature did not exist at 315 min, the pressurizer level measurement indicates that the pressurizer was totally filled with liquid after that time, thus the subcooling assumption of the pressurizer fluid should be reasonable after 315 min. A comparison of integrated mass-flow is shown in Figure 32, the best-estimate case resulting in lower mass-flows than the limiting case beyond 206 min, as expected from decreased subcooling effects. Figures 33 and 34 show calculated mass-flowrates for the best-estimate case and the maximum flow limiting case, respectively.

P. Kuan, EG&G Idaho, calculated discharge flow out of the PORV based on an approximation that the flowrate is proportional to the square root of the primary system pressure and is obtained for several subdivided periods of the accident time.<sup>9</sup> He assumed saturated steam and subsequent saturated water flow from 220 min to 318 min. According to his calculation, the integrated mass-flow at 800 min into the accident is  $8.01 \times 10^5$  kg, which is some 10% smaller than the  $9.20 \times 10^5$  kg obtained in the present best-estimate calculation. This present value is considered adequate when compared with other reported values based on the measured level data of the Borated Water Storage Tank.<sup>13</sup>



PS11-WHT-1187-18

Figure 32. Comparison of calculated integrated mass-flow between the best estimate case and the limiting case.



PS11-WHT-1187-08

Figure 33. Calculated mass flowrates for the best estimate case.

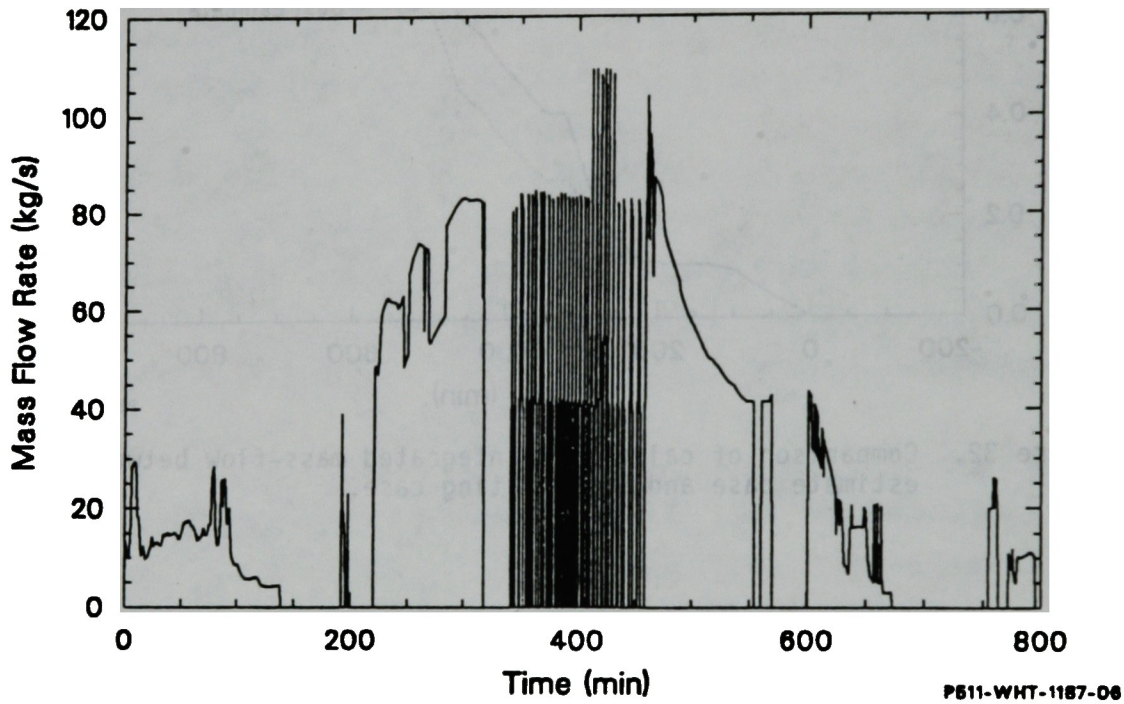


Figure 34. Calculated mass flowrates for the limiting case.

## 6. UNCERTAINTY ANALYSIS

Performing a classical uncertainty analysis on the estimated PORV flowrates is extremely difficult. As a result, it was decided to provide an estimate of the uncertainty based upon engineering judgment. Previous uncertainty analyses have shown that engineering judgment is a valid method for estimating uncertainties when more rigorous methods are impractical, and usually results in estimates that are consistent with a 95% confidence level. The major sources of uncertainty in the PORV mass flowrate estimates are considered to be:

- Uncertainties in the input data for the calculation, such as the discharge coefficient and assumptions in the model about subcooled conditions at the PROV. A total uncertainty in these parameters of  $\pm 15\%$  is estimated. This is the dominant uncertainty component.
- The uncertainty in the steam velocity through the pressurizer, as calculated from the Wilson correlation using the pressurizer level, is estimated at  $\pm 10\%$ .
- Uncertainties in the critical flowrates obtained from the Davis critical flow tables is estimated at  $\pm 5\%$ .

Combining these uncertainty components using the Root-Sum-Square method results in a total uncertainty estimate of  $\pm 20\%$ .

## 7. CONCLUSIONS

A model has been developed for estimating the fluid conditions at the PORV during the TMI-2 accident. This model allows the flowrate through the PORV to be calculated for those periods in which the PORV block valve was open. The fluid conditions model is based upon Wilson's correlation between steam velocity through the pressurizer vessel and the void fraction in the pressurizer as obtained from the liquid level measurement, and includes effects of fluid subcooling. The developed model was tested using data obtained in a series of semiscale experiments, and resulted in measured flowrates (error in total calculated mass flow was less than 8%). Following checkout of the model against the Semiscale data, the model was applied to TMI-2 during the first 795 min of the accident (at this time the PRV block valve was closed and remained close thereafter). Results from this analysis have been presented, with a total mass loss from the TMI-2 primary system, through the PORV, of 920,000 kg  $\pm$ 20% during the accident. These results are considered to be the current best estimate of the PRV flowrates during the TMI-2 accident.

## B. REFERENCES

1. D. W. Golden, TMI-2 Analysis Exercise, prepared for the U.S. Nuclear Regulatory Commission, May 1987.
2. J. C. M. Leung, Analysis of Thermal Hydraulic Behavior During TMI-2 LOCA, ANL/LWR/SAF 80-4, October 1980.
3. C. B. Davis, "IBM PC Critical Flow Tables," EG&G Idaho Interoffice Correspondence, CBD-3-86, September 1986.
4. G. B. Wallis, One Dimensional Two-Phase Flow, McGraw Hill Inc., New York, 1969.
5. K. H. Sun, et al., "The Prediction of Two-Phase Mixture Level and Hydrodynamically-Controlled Dryout Under Low Flow Conditions," Int. J. Multiphase Flow, 7, No. 5, pp. 521-543, 1981.
6. K. E. Sackett and L. B. Clegg, Experiment Data Report of Semiscale MOD-2B Power Loss Test Series (Tests S-PL-1, -2, and -3), NUREG/CR-3419, August 1983.
7. J. R. Wolf, et al., Analysis of the Semiscale Mod-2B Power Loss Experiment S-PL-3, EGG-SEMI-6429, October 1983.
8. Nuclear Safety Analysis Center, Analysis of Three Mile Island--Unit 2 Accident, NSAC-80-1, March 1980.
9. P. Kuan, "Study of Pressurizer Outflow to the Containment During the TMI-2 Accident," EG&G Idaho Interoffice Correspondence, PK-15-86, December 1986.
10. EPRI PWR Safety and Relief Valve Test Program: Safety and Relief Valve Test Report, EPRI-NP-2628-sr, December 1982.
11. J. L. Anderson, Analysis of TMI-2 Pressurizer Level Indications, EGG-TMI-7100, January 1986.
12. Robert E. Henry, et al., Core Relocation Phenomenology, Internal Report of Fauske & Associates Inc., 1985.
13. Investigation into the March 28, 1979 Three Mile Island Accident by Office of Inspection and Enforcement, NUREG-0600, August 1979.



